Contribution from the Laboratoire de Physique Quantique (CNRS, UA 505) and Laboratoire des Organométalliques (CNRS, UA 477), Université Paul Sabatier, 31062 Toulouse Cedex, France

Binding Phosphinidenes to Transition-Metal Fragments

GEORGES TRINQUIER*† and GUY BERTRAND‡

Received December 21, 1984

Phosphinidenes can be stabilized through internal π conjugation as in phosphinophosphinidenes, R_2P-P. Such species should be even more efficiently stabilized through transition-metal complexation. This work is a detailed analysis of orbital interactions occurring when H_2P-P is bound (η^1) to various ML_n metallic fragments. The most favorable fragments allow both the donation of the two lone pairs (σ and π) of the terminal phosphorus and the back-donation of a metal d pair into the empty π^*_{P-P} orbital. This is accomplished with the 14-electron species d^4 C_{4v} ML_5, d^6 C_{2v} ML_4, and d^8 C_{3v} ML_3 and, to a lesser extent, with d^6 C_{2v} ML_3, d^8 C_{2v} ML_2 (12 e), and d^6 C_{3v} ML_4 (14 e). Tetrahedral complexes with a d^8 ML_3 unit such as $Fe(CO)_3$ produce the strongest binding. This study is extended to other phosphinidene ligands, $(H_2N)_2P-P$, H_2N-P, H_3C-P, and C_6H_5-P, and to nitrene ligands, H_2N-N and H_2P-N. Bridging is examined in $H_2P-P(ML_5)_2$ dinuclear complexes.

I. Introduction

Nitrenes and phosphinidenes are known as transient species, and their chemistry has been widely studied.[1] These species can be stabilized through complexation on transition-metal fragments. However, a difference appears between nitrenes and phosphinidenes concerning the mode of binding to the metal centers. Although some terminal nitrene complexes are known,[2] to date the only known stable phosphinidene complexes involve bridging (i.e. μ_2, μ_3, or μ_4) phosphinidenes.[3] Complexes involving terminal phosphinidenes have proven to be only transient species.[4-7]

A question arises as to whether there is a predisposition for phosphinidenes to behave only as polybridging ligands, inasmuch as the parent valence isoelectronic carbyne ligand (that we consider as $R-\overset{+}{C}:^-$ for electron count purposes) also can give both terminal or bridged complexes.[8]

The present paper presents a theoretical analysis of the bonding occurring in complexes formed by terminal phosphinidenes with various metallic fragments, eventually suggesting the most suitable transition-metal fragments that could give such stable terminal complexes.

Like nitrenes, phosphinidenes can be stabilized by putting π-donor substituents in the α position. This strategy made possible the synthesis of relatively stable aminonitrenes[9] and phosphinonitrene.[10] The singlet states are more stabilized than the triplet states, so that the general propensity to triplet ground states can be upset if a sufficient π-delocalization possibility is given.[11] We can illustrate this by giving the triplet-singlet splitting in some nitrenes (a negative sign means a singlet ground state):

H-N	36 kcal/mol[12]
CHO-N	31 kcal/mol[13]
C_6H_5-N	4 kcal/mol[14]
H_2P-N	−6 kcal/mol[11]
H_2N-N	−15 kcal/mol[15]

In our study we shall consider model phosphinidenes that are already stabilized by internal π conjugation. We have chosen to focus on phosphinophosphinidene, $H_2P—P$, which is the isomerical alternative to diphosphene HP=PH. Diphosphenes have now been observed either as isolated species or in complexed forms on transition metal centers.[16,17] The H_2P-P ligand is taken in a planar singlet form (which was calculated to lie 29 kcal/mol above *trans*-diphosphene).[17d] We shall see that, at our level of analysis, a triplet configuration for the ligand would change the bonding very little. Furthermore, it is presumed that a stable phosphinophosphinidene is likely to bear stabilizing π-donor (or π-acceptor) substituents, thus favoring a planar singlet ground state. Other phosphinidene ligands will be considered later: H_2N-P, CH_3-P, and Ph-P. The study will be extended to the nitrene ligands H_2N-N and H_2P-N. Finally, we shall consider bridging in the simplest case: μ_2 dinuclear models.

We base our study on one-electron effects obtained from extended Hückel calculations. Orbital interaction diagrams resulting from fragment molecular orbital (FMO) analyses will be largely used. The extended Hückel parameters and the geometrical

† Laboratoire de Physique Quantique.
‡ Laboratoire des Organométalliques.

(1) (a) Lwowski, W. "Nitrenes"; Wiley-Interscience: New York, 1970. (b) Schmidt, U. *Angew. Chem., Int. Ed. Engl.* **1975**, *14*, 523.
(2) (a) Lwowsky, W. In "Reactive Intermediates"; Jones, M., Moss, R., Eds.; Wiley: New York, 1978; Chapter 6. (b) Nugent, W. A.; Haymore, B. L. *Coord. Chem. Rev.* **1980**, *31*, 23. (c) Dehnicke, K.; Strähle, J. *Angew. Chem., Int. Ed. Engl.* **1981**, *20*, 413. (d) Mahy, J. P.; Battioni, P.; Mansuy, D.; Fisher, J.; Weiss, R.; Mispelter, J.; Morgenstern-Badarau, I.; Gans, P. *J. Am. Chem. Soc.* **1984**, *106*, 1699. (e) Maatta, E. A. *Inorg. Chem.* **1984**, *23*, 2560. (f) Hegedus, L. S.; Kramer, A. *Organometallics* **1984**, *3*, 1263. (g) Cotton, F. A.; Duraj, S. A.; Roth, W. J. *J. Am. Chem. Soc.* **1984**, *106*, 4749. (h) Marchi, A.; Rossi, R.; Duatti, A.; Magon, L.; Casellato, U.; Graziani, R. *Transition Met. Chem. (Weinheim, Ger.)* **1984**, *9*, 299. (i) Lin, Y. C.; Knobler, C. B.; Kaesz, H. D. *J. Organomet. Chem.* **1981**, *213*, C41. (j) White, R. E.; McCarthy, M. B. *J. Am. Chem. Soc.* **1984**, *106*, 4922. (k) Hsieh, T. C.; Gebreyes, K.; Zubieta, J. *J. Chem. Soc., Chem. Commun.* **1984**, 1172. (l) Brennan, J. G.; Andersen, R. A. *J. Am. Chem. Soc.* **1985**, *107*, 514. (m) Chan, D. M. T.; Fultz, W. C.; Nugent, W. A.; Roe, D. C.; Tulip, T. H. *J. Am. Chem. Soc.* **1985**, *107*, 251. (n) Gross, M. E.; Johnson, C. E.; Maroney, M. J.; Trogler, W. C. *Inorg. Chem.* **1984**, *23*, 2968. (o) Chatt, J.; Dosser, R. J.; King, F.; Leigh, G. J. *J. Chem. Soc., Dalton Trans.* **1976**, 2435. (p) For an MO treatment of transition metal complexes with ligands N, NN, or NNR, see: Dubois, D. L.; Hoffmann, R. *Nouv. J. Chim.* **1977**, *1*, 479.
(3) (a) For a review, see: Marinetti, A. Thesis, Université Pierre-et-Marie-Curie, Paris, 1984. (b) Duttera, M. R.; Day, V. W.; Marks, T. J. *J. Am. Chem. Soc.* **1984**, *106*, 2907. (c) Kwek, K.; Taylor, N. J.; Carty, A. J. *J. Am. Chem. Soc.* **1984**, *106*, 4636. (d) Seyferth, D.; Withers, H. P., Jr. *Organometallics* **1982**, *1*, 1294. (e) Williams, G. D.; Geoffroy, G. L.; Whittle, R. R. *J. Am. Chem. Soc.* **1985**, *107*, 729. (f) For closo 6-vertex clusters containing two trans μ_4-PhP units, see: Halet, J. F.; Hoffmann, R.; Saillard, J. Y. *Inorg. Chem.* **1985**, *24*, 1695.
(4) Marinetti, A.; Mathey, F.; Fischer, J.; Mitschler, A. *J. Chem. Soc. Chem. Commun.* **1982**, 667.
(5) Marinetti, A.; Mathey, F.; Fischer, J.; Mitschler, A. *J. Am. Chem. Soc.* **1982**, *104*, 4484.
(6) (a) Marinetti, A.; Mathey, F. *Organometallics* **1984**, *3*, 456. (b) Marinetti, A.; Mathey, F. *Organometallics* **1984**, *3*, 1492.
(7) Nakazawa, H.; Buhro, W. E.; Bertrand, G.; Gladysz, J. A. *Inorg. Chem.* **1984**, *23*, 3431.
(8) (a) Purcell, K. F.; Kotz, J. C. "Inorganic Chemistry"; W. B. Saunders: Philadelphia, 1977; p 863. (b) Collman, J. P.; Hegedus, L. S. "Principles and Applications of Organotransition Metal Chemistry"; University Science Books: Mill Valley, CA 1980; p 103. (c) Clauss, A. D.; Shapley, J. R.; Wilker, C. N.; Hoffmann, R. *Organometallics* **1984**, *3*, 619. (d) Ros, J.; Solans, X.; Font-Altaba, M.; Mathieu, R. *Organometallics* **1984**, *3*, 1014. (e) Carriedo, G. A.; Howard, J. A. K.; Stone, F. G. A. *J. Chem. Soc., Dalton Trans.* **1984**, *8*, 1555. Jeffery, J. C.; Laurie, J. C. V.; Moore, I.; Razay, H.; Stone, F. G. A. *Ibid.* **1984**, *8*, 1563. Jeffery, J. C.; Moore, I.; Stone, F. G. A. *Ibid.* **1984**, *8*, 1571. Jeffery, J. C.; Moore, I.; Razay, H.; Stone, F. G. A. *Ibid.* **1984**, *8*, 1581. Carriedo, G. A.; Howard, J. A. K.; Marsden, K.; Stone, F. G. A.; Woodward, P. *Ibid.* **1984**, *8*, 1589. Carriedo, G. A.; Jeffery, J. C.; Stone, F. G. A. *Ibid.* **1984**, *8*, 1597. Behrens, U.; Stone, F. G. A. *Ibid.* **1984**, *8*, 1605.
(9) See, for instance: Sylwester, A. P.; Dervan, P. B. *J. Am. Chem. Soc.* **1984**, *106*, 4648 and reference 4 in this work.
(10) (a) Sicard, G.; Baceiredo, A.; Bertrand, G.; Majoral, J. P. *Angew. Chem., Int. Ed. Engl.* **1984**, *23*, 459. (b) Baceiredo, A.; Bertrand, G.; Majoral, J. P.; El Anba, F.; Manuel, G. *J. Am. Chem. Soc.* **1985**, *107*, 3945.
(11) Trinquier, G. *J. Am. Chem. Soc.* **1982**, *104*, 6969.
(12) Huber, K. P.; Herzberg, G. "Constants for Diatomic Molecules"; Van Nostrand-Reinhold: New York, 1979.
(13) Mavridis, A.; Harrison, J. F. *J. Am. Chem. Soc.* **1980**, *102*, 7651.

0020-1669/85/1324-3842$01.50/0

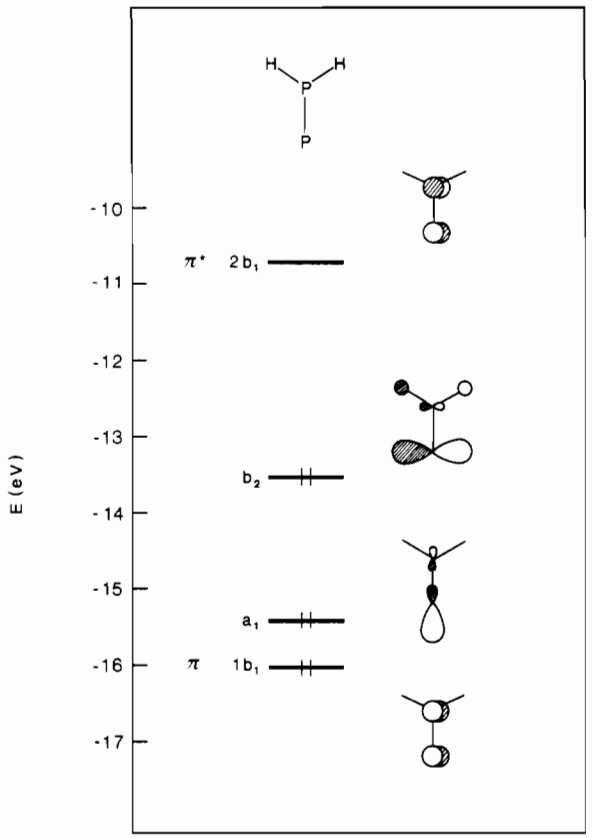

Figure 1. Relevant molecular orbitals of the phosphinophosphinidene ligand.

assumptions used in this work are given in the Appendix.

Before considering in detail the bonding abilities of different classes of metallic fragments toward H_2P–P—starting with those derived from the octahedron in which one, two, and then three ligands are successively removed—we shall examine the electronic structure of our model ligand. The four relevant orbitals that can be involved in the bonding to the metal are plotted in Figure 1. The lower MO of this set, $1b_1$, corresponds to the phosphino π lone pair, conjugated with a p orbital of the neighbor phosphorus atom (**1**). In an extended Hückel calculation, both phosphorus

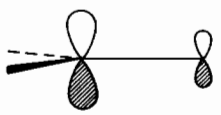

1

atoms bear the same coefficients as occurs also for the antibonding counterpart $2b_1$ of this π system (see Figure 1). Actually, as illustrated by ab initio calculations, there is a dissymetry and $1b_1$ is more the phosphino lone pair whereas $2b_1$ is more the vacant

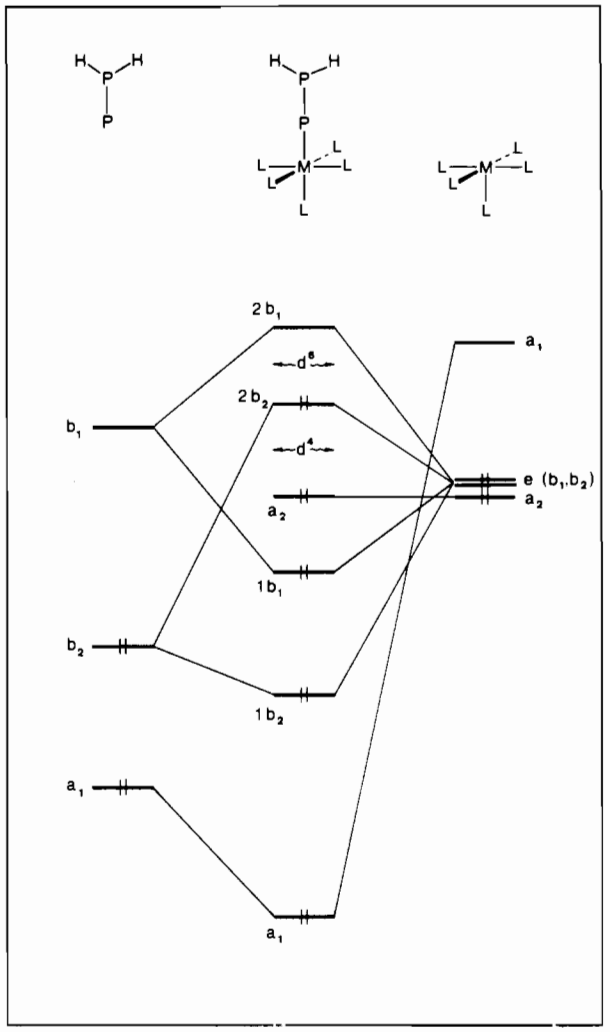

Figure 2. Schematized interaction diagram for d^6 H_2PP–ML_5.

p atomic orbital on the terminal phosphorus. Since $1b_1$ is not located mainly on the terminal phosphorus, this orbital will not be involved in the η^1 bonding but will be involved in η^2 bonding.

Next, we have two orbitals corresponding to the phosphinidene lone pairs: a_1 is a sp-hybridized σ lone pair pointing away from the P–P bond as schematized in **2**. b_2, the HOMO, is a p lone pair (**3**). Figure 1 shows that b_2 has a component on the

2 **3**

phosphino group. In fact, this orbital should also have a significant coefficient on a d orbital of the adjacent phosphorus, as has been reported elsewhere for H_2P–N.[11] This interaction is not taken into account at our level since we do not include d orbitals in the basis sets for main-group atoms.

The LUMO, $2b_1$, is the remaining vacant p atomic orbital of the terminal phosphorus (**4**). It is the antibonding counterpart of $1b_1$. This orbital may receive electrons from a metal, thus contributing to back-bonding.

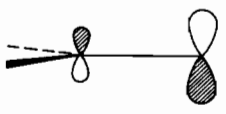

4

It can be pointed out in Figure 1 that if b_2 is empty, the orbital pattern of singlet vinylidene R_2C=C: is obtained. Therefore, from simple electron-count considerations, the various known d^m ML_n–CCR_2 systems[18] (e.g. with a d^6 ML_5 fragment) suggest the

(14) Drzaic, P. S.; Brauman, J. I. *J. Am. Chem. Soc.* **1984**, *106*, 3443. Drzaic, P. S.; Brauman, J. I. *J. Phys. Chem.* **1984**, *88*, 5285.

(15) (a) Davis, J. H.; Goddard, W. A., III. *J. Am. Chem. Soc.* **1977**, *99*, 7111. (b) For a review on singlet–triplet separations in nitrenes, see: Davidson, E. R. In "Diradicals"; Borden, W. T., Ed.; Wiley: New York, 1982; Chapter 2, p 73.

(16) (a) Cowley, A. H. *Polyhedron* **1984**, *3*, 389. (b) Cowley, A. H.; Kilduff, J. A.; Lasch, J. G.; Mehrotra, S. K.; Norman, N. C.; Pakulski, M.; Whittlesey, B. R.; Atwood, J. L.; Hunter, W. E. *Inorg. Chem.* **1984**, *23*, 2582. (c) Cowley, A. H.; Kilduff, J. E.; Lasch, J. G.; Pakulski, M.; Ando, F.; Wright, T. C. *Organometallics* **1984**, *3*, 1044. (d) See also, for a review: Ranaivonjatovo, H. J. Thèse de troisième cycle, Université Paul Sabatier, Toulouse, France, 1984.

(17) For theoretical studies on diphosphene HP=PH, see: (a) Yoshifuji, M.; Shibayama, K.; Inamoto, N. *J. Am. Chem. Soc.* **1983**, *105*, 2495. (b) Lee, J. G.; Cowley, A. H.; Boggs, J. E. *Inorg. Chim. Acta* **1983**, *77*, L61. (c) Galasso, V. *Chem. Phys.* **1984**, *83*, 407. (d) Ha, T. K.; Nguyen, M. T.; Ruelle, P. *Chem. Phys.* **1984**, *87*, 23.

Table I. Summary of the Results of Extended Hückel Calculations for Complexes of H_2P–P with Nonfavorable Fragments

fragments	ΔE, eV	tot. overlap pop. P–M	tot. overlap pop. P–P	gross charge transfer, e P → M	gross charge transfer, e P ← M	Δ(HOMO–LUMO), eV
WH_5^{5-}	2.88	0.89	1.06		0.56	1.06
$W(CO)_5$	1.21	0.81	1.16		0.03	0.90
WH_4Cl^{5-}	3.34	0.88	1.03		0.64	0.99
$W(CO)_4Cl^-$	1.27	0.79	1.12		0.25	0.34
$PtCl_3^-$, η^2	0.63	0.28 0.30	1.09		0.42	1.83
$PtCl_3^-$, η^1 eclipsed	0.93	0.74	1.23	0.12		1.02
$PtCl_3^-$, η^1 staggered	1.87	0.84	1.25	0.34		2.11

possibility for d^{m-2} ML_n–PPR_2 corresponding systems (e.g. with a d^4 ML_5 fragment).

II. Binding to ML_5 Fragments

$W(CO)_5$ is a metallic fragment that is easy to generate by irradiation of $W(CO)_6$ and is widely used in organo–transition-metal synthesis.[3-6] Is this fragment a good candidate for binding R_2P–P? The orbital interaction diagram for such an adduct is schematized in Figure 2. The classical orbital pattern for d^6 ML_5 is "three below one", or a remainder of the t_{2g} set of d orbitals in an octahedral complex, and a hybrid pointing in the z direction (**5**).[19,20] Although this ML_5 fragment has C_{4v} symmetry, it is

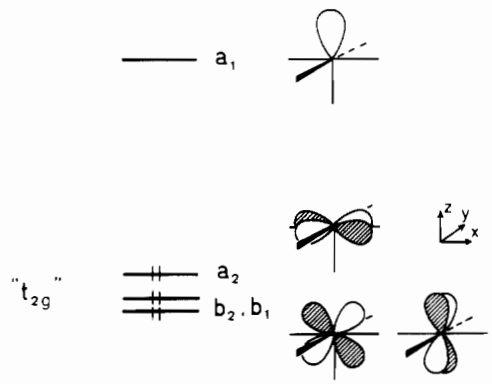

5

more convenient to use the notations of the C_{2v} subgroup since the whole complex has C_{2v} symmetry. When R_2P–P is fixed to ML_5, occupied a_1 and empty b_1 orbitals of our ligand encounter, on the metal fragment, both an empty a_1 orbital and an occupied b_1 orbital to give two stabilizing two-orbital two-electron interactions. On the other hand, since the b_2 orbital of R_2P–P and the b_2 orbital of ML_5 are both occupied, the resulting b_2 orbitals (indicated $1b_2$ and $2b_2$ in Figure 2) will both be occupied too, giving a destabilizing two-orbital four-electron interaction. The effect of all these interactions is stabilizing. A binding energy of 2.9 eV is obtained when H_2P–P is coordinated on WH_5^{5-} and 1.2 eV on $W(CO)_5$. Note on Figure 2 that a triplet configuration for H_2P–P, i.e. both b_2 and b_1 being monooccupied, would not change anything in the scheme of the bonding; it would only increase the binding energy.

There is a way to cancel the b_2–b_2 repulsive interaction. Bending the ligand minimizes the overlap between the two b_2 orbitals due to sp^2 rehybridization of the b_2 phosphinidene lone pair (**6**). This bending, which minimizes the lone-pair repulsions, should be observed for any stable complex with d^6ML_5 fragments.

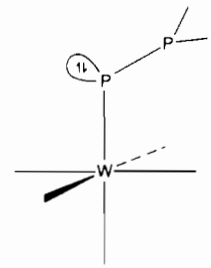

6

One can see in Figure 2 that there is another way of making the interaction between the b_2 orbitals stabilizing. Obviously if the ML_5 fragment bears 4 d electrons instead of 6, the $2b_2$ orbital will be empty. So a d^4 electron count for the ML_5 fragment ensures the maximum of bonding interactions. This is accomplished with WH_5^{3-} and $W(CO)_5^{2+}$, which give stronger binding energies than their corresponding d^6 fragments: 6.0 eV and 4.3 eV, respectively. Other possible d^4 ML_5 species are $Ti(CO)_5$ or $V(Cp)(CO)_2$, giving **7**, since η^5-$C_5H_5^-$ acts as a *fac*-L_3 set.[19] The binding energy in **7** is calculated at 4.3 eV.

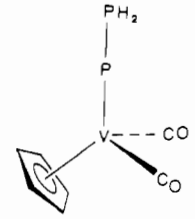

7

To make the comparisons between all the fragments more quantitative, we shall use, besides the binding energies, some other indexes. First, the total overlap population between the metal atom and the phosphinidene end will be a good hint of the strength of the P–M bond. It varies in the same way as the binding energy between H_2P–P and ML_n. The total overlap population between the two phosphorus atoms in H_2P–P is 1.34 for the isolated molecule. Its value when H_2P–P is complexed to the metal mainly reflects the extent to which the empty b_1 orbital of H_2P–P is involved in the P–M bonding; i.e., it becomes populated by receiving electrons from some metal orbital of the same symmetry. The P–P overlap population does not follow the binding energy and does not represent the strength of the P–M bond. It parallels the strength and the multiplicity of the P-P bond, which has some double and even triple character in the isolated molecule. This multiplicity is more or less reduced by populating the empty P–P antibonding b_1 orbital when H_2P–P is bonded to our metal fragments. This weakening of the P–P bond, described by the corresponding overlap population, is not without interesting possible consequences for the chemist.

Another result that is given by our population analyses is the whole electronic transfer between the ligand and the metallic part. When the three main interactions involving the three high-lying orbitals of H_2P–P are all bonding, a_1 and b_2 pairs are partly

(18) (a) Stang, P. J. *Chem. Rev.* **1978**, *78*, 383. (b) Fehlhammer, W. P.; Stolzenberg, H. In "Comprehensive Organometallic Chemistry"; Wilkinson, G., Stone, F. G. A., Abel, E. W., Eds.; Pergamon Press: Oxford, England, 1982; Vol. 4, p 529. Bennet, M. A.; Bruce, M. I.; Matheson, T. W. *Ibid.* pp 691, 821. Adams, R. D.; Selegue, J. P. *Ibid.* p 967. (c) Bruce, M. I.; Swincer, A. G. *Adv. Organomet. Chem.* **1983**, *22*, 59. (d) "Transition Metal Carbene Complexes"; Verlag Chemie: Weinheim, West Germany, 1983. (e) Wolf, J.; Werner, H.; Serhadli, O.; Ziegler, M. L. *Angew. Chem., Int. Ed. Engl.* **1983**, *22*, 414. (f) Werner, H.; Wolf, J.; Zolk, R.; Schubert, U. *Angew. Chem., Int. Ed. Engl.* **1983**, *22*, 981. (g) Werner, H.; Wolf, J.; Müller, G.; Krüger, C. *Angew. Chem., Int. Ed. Engl.* **1984**, *23*, 431. (h) Consiglio, G.; Bargenter, F.; Darpin, C.; Morandini, F.; Lucchini, V. *Organometallics* **1984**, *3*, 1146. (i) Mott, G. N.; Carty, A. J. *Inorg. Chem.* **1983**, *22*, 2726. (j) Carty, A. J.; Taylor, N. J.; Sappa, E.; Tiripicchio, A. *Inorg. Chem.* **1983**, *22*, 1871. (k) Bruce, M. I.; Hambley, T. W.; Snow, M. R.; Swincer, A. G. *Organometallics* **1985**, *4*, 501. (l) Casey, C. P.; Miles, W. H.; Fagan, P. J.; Haller, K. J. *Organometallics* **1985**, *4*, 559. For MO treatments, see: (m) Schilling, B. E. R.; Hoffmann, R.; Lichtenberger, D. L. *J. Am. Chem. Soc.* **1979**, *101*, 586. (n) Kostic, N. M.; Fenske, R. F. *Organometallics* **1982**, *1*, 974.

(19) Hoffmann, R. *Angew. Chem., Int. Ed. Engl.* **1982**, *21*, 711.

(20) The orbitals for all the metal carbonyl fragments are detailed in: Elian, M.; Hoffmann, R. *Inorg. Chem.* **1975**, *14*, 1058.

Table II. Summary of the Results for Complexes of H_2P–P with Favorable Fragments

types of fragment	fragments	ΔE, eV	tot. overlap pop. P–M	tot. overlap pop. P–P	gross charge transfer, e P → M	gross charge transfer, e P ← M	Δ(HOMO–LUMO), eV
C_{4v} d^4 ML_5	WH_5^{3-}	6.02	1.29	1.02		0.14	1.57
	$W(CO)_5^{2+}$	4.32	1.06	1.13	0.49		1.79
	$V(Cp)(CO)_2$	4.25	0.98	1.11	0.24		1.87
C_{2v} d^6 ML_3	NiF_3^+	4.94	0.84	1.35	1.91		1.30
	$PtCl_3^+$	3.16	1.03	1.24	0.85		0.75
	$W(CO)_3$	4.35	1.14	1.13	0.13		0.47
C_{2v} d^6 ML_4	WH_4^{4-}	5.54	1.34	1.01		0.23	1.84
	$W(CO)_4$	5.10	1.19	1.11	0.17		1.52
	$Cr(CO)_4$	4.81	1.14	1.16	0.45		1.89
	$Fe(CO)_4^{2+}$	3.98	0.97	1.22	0.82		2.15
	$Mn(Cp)(CO)$	5.37	1.21	1.12	0.25		2.41
	$Fe(Cp)(CO)^+$	4.27	1.06	1.17	0.42		2.65
	$Fe(\eta^6\text{-}C_6H_6)(CO)^{2+}$	4.50	1.07	1.18	0.54		2.25
C_{2v} d^8 ML_2	$Fe(CO)_2$	4.42	1.15	1.22	0.69		1.51
	$Ni(CN)_2$	2.61	0.90	1.25	0.57		1.31
	$Ni(Cl)_2$	2.95	0.94	1.25	0.64		0.82
C_{3v} d^8 ML_3	$Fe(CO)_3$	6.12	1.24	1.05		0.02	2.48
	$Fe(C_6H_6)$	6.01	1.26	1.05		0.05	2.19
	$Fe(Cp)^-$	6.30	1.23	1.01		0.21	2.49
	$Co(Cp)$	4.16	1.02	1.12	0.06		0.99
C_{3v} d^6 ML_4	NiF_4	3.82	0.80	1.35	2.02		1.03

transferred to the metal, while b_1 receives part of an electron pair from the metal. The balance between these three main electronic transfers will give an overall charge transfer that is generally in the P → M direction, but which can be in the P ← M direction or close to zero due to an eventual cancellation of transfers in the two directions. Everytime we get a near-zero or P ← M resulting charge transfer, the b_1 orbital (which is P–P antibonding) becomes significantly populated, and at the same time the P–P overlap population should and does decrease.

Last, we shall use the HOMO–LUMO gap, which is, in our approach, a rough index for the kinetic stability of the molecule, especially as we consider low-spin complexes. One must be cautious, since even in nonmetallic compounds, some triplet species can be viable with a near-zero HOMO–LUMO gap obtained at our extended Hückel level. All through this work, we say that the larger the binding energy and HOMO–LUMO gap, the more viable the complex.

ML_5 fragment data are given in Table I (top) for the "unfavorable" d^6 ML_5 fragments and in Table II (top) for the "favorable" d^4 ML_5 fragments. The stronger bonding capabilities of d^4 ML_5 over d^6 ML_5 appear clearly from these two tables. In the d^6 complexes the prevailing bonding interaction involves the b_1 orbitals, giving a whole P ← M electron transfer. In the d^4 complexes the three bonding interactions result in a whole P → M transfer with $W(CO)_5^{2+}$ and $V(Cp)(CO)_2$ while a P ← M transfer with WH_5^{3-} is seen. This means that in WH_5^{3-} (which is d^4) the b_1–b_1 interaction prevails among the three main bonding interactions. This is because of the b_1–b_1 energy matching, which is better with WH_5^{3-} than with the other ML_5 fragments. Accordingly, the P–P bond is more weakened in H_2PP–WH_5^{3-} than in H_2PP–$W(CO)_5^{2+}$ or H_2PP–$V(Cp)(CO)_2$, as can be seen from the P–P overlap population given in Table II (top).

According to our MO analysis, a viable complex of phosphinidene with an ML_5 metallic part should have, therefore, a d^4 electron count rather than a d^6 count. With a d^4 electron count, the metal can accept the donation of the two lone pairs from the phosphinidene end. By so doing, it surrounds itself with 18 electrons (4 + (2 × 2) + (5 × 2)), while it gives in turn a d lone pair to the phosphorus atom. This bonding scheme will hold with all the "favorable" fragments. In the best cases, one could write a formally triple bond between P and M. The P–P bond, which was formally double (and, to some extent triple) becomes single:

$$R_2P{=}P + ML_n \rightarrow R_2P{-}P{\equiv}ML_n$$

On the other hand the complex R_2P–P with an "unfavorable" d^6ML_5 fragment can be written with a formally double P–M bond. These multiplicities however differ according to the metal, the ligands, and the substituents. For this reason we prefer to use the more flexible single-bond notation.

To the extent that the bonding scheme is basically the same for R_2P–P or any phosphinidene ligand (as we shall see), some experimental results support our conclusions. Transient complexes of phosphinidenes with d^6 ML_5 fragments have been put in evidence but they are nonviable species which rearrange or react easily:

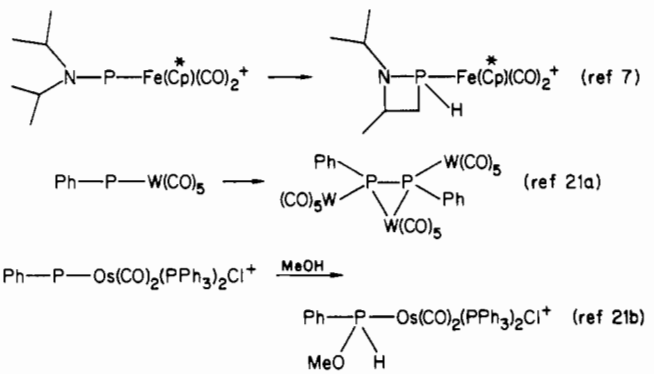

In the recently reported stable complex $Cp(CO)_2Mo$–P–C–$(SiMe_3)_2$,[21c] the ligand can be considered to be $P{-}CR_2^+$ or $P{-}CR_2^-$. With the latter form, which is valence isoelectronic with $P{-}PR_2$, the metallic part is a d^4 ML_5 fragment. Moreover, we know that in nitrene chemistry, transition-metal complexes with a d^4 ML_5 unit are stable species.[2b,h,p]

A substituent effect can be used to decrease the b_2–b_2 destabilizing interaction in the d^6 ML_5 complexes. A π-donor ligand trans to PPH_2 should push up the d_{xz} and d_{yz} orbitals of the metal e set. The resulting increased gap between the b_2 levels should induce a decreased overall destabilization. Actually the binding energies are larger for the WH_4Cl^{5-} and $W(CO)_4Cl^-$ fragments than for the WH_5^{5-} and $W(CO)_5$ fragments (see Table I), but the effect is tiny. Since the b_1 metal orbital has also been pushed up, the transfer of electrons from the metal to the ligand, which is due to the b_1–b_1 mixing, is significantly increased, as can be seen in Table I. This last effect holds for the d^4 electron count as well.

III. Binding to C_{2v} ML_3 Fragments

Let us consider now a fragment that is directly derived from d^4 ML_5. The isolobal analogy[19] tells us that the bonding with d^6

(21) (a) Marinetti, A.; Mathey, F.; Fischer, J.; Mitschler, A. *Organometallics*, in press. (b) Bohle, D. S.; Roper, W. R. *J. Organomet. Chem.* **1984**, *273*, C4. (c) Cowley, A. H.; Norman, N. C.; Quashie, S. *J. Am. Chem. Soc.* **1984**, *106*, 5007.

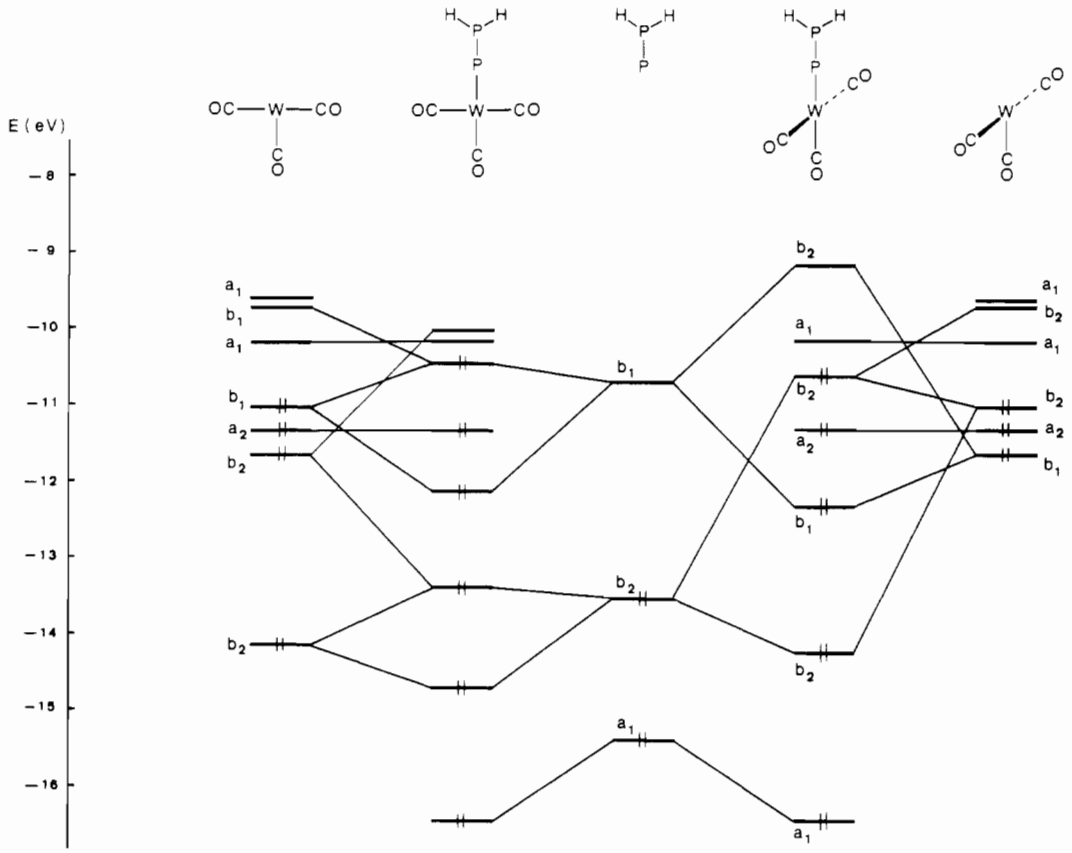

Figure 3. Interaction diagrams for H_2PP–$W(CO)_3$ in the eclipsed (left) and staggered (right) forms.

Table III. Summary of the Results for Complexes of H_2P–P with d^6 C_{2v} ML_3 Fragments

fragments		ΔE, eV	tot. overlap pop. P–M	tot. overlap pop. P–P	gross charge transfer, e P → M	gross charge transfer, e P ← M	Δ(HOMO–LUMO), eV
$W(CO)_3$	eclipsed	3.25	1.24	0.96		0.11	0.29
	staggered	4.35	1.14	1.13	0.13		0.47
NiF_3^+	eclipsed	4.92	0.84	1.35	2.07		1.31
	staggered	4.94	0.84	1.35	1.91		1.04
$PtCl_3^+$	eclipsed	2.77	1.04	1.22	0.89		1.02
	staggered	3.16	1.03	1.24	0.85		0.75

C_{2v} ML_3 should not be that different from the bonding with d^4 ML_5 (**8**).

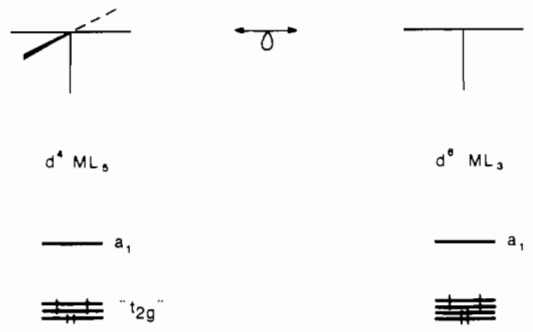

8

We have thus studied the fragments $W(CO)_3$, NiF_3^+, and $PtCl_3^+$. The binding energy with $W(CO)_3$ is quite comparable to that with $W(CO)_5^{2+}$, as can be seen in Table II. However, the HOMO–LUMO gap is much weaker. Figure 3 shows the orbital interaction diagram for the two forms of H_2PP–$W(CO)_3$. In the $W(CO)_3$ fragment there is another low-lying b_1 (or b_2) empty level, which has the same symmetry as the HOMO and will therefore give secondary interactions. In the eclipsed planar complex these levels interact with the empty b_1 orbital of H_2PP (Figure 3, left). In the staggered nonplanar complex these levels interact with the occupied b_2 orbital of H_2PP (Figure 3, right). In both complexes the result of this three-orbital interaction gives a relatively high-lying HOMO, which, combined with the low-lying a_1 LUMO from $W(CO)_3$, leads to a narrow HOMO–LUMO gap, especially in the eclipsed planar form. The binding energy in the planar form is only 3.25 eV vs. 4.35 eV in the staggered nonplanar form. This difference is mainly due to another secondary interaction, which lessens the b_2–b_2 interaction in the eclipsed planar form.

Although we have both a good binding energy and a good P–M overlap population for staggered nonplanar H_2PP–$W(CO)_3$, the narrow HOMO–LUMO gap should significantly restrict the viability of such a complex.

With the NiF_3^+ fragment, the interaction diagrams are simplified since, due to the deepness of the nickel 3d levels, (1) no important secondary interaction occurs and (2) there is no b_1–b_1 bonding interaction. This implies that, in such a species, the P–Ni bond will be less multiple and will be dominated by P → Ni electronic transfers. The interaction diagrams for eclipsed and staggered H_2PP–NiF_3^+ show that the b_2–b_2 stabilizing interaction is slightly larger in the staggered form, but it also gives a smaller HOMO–LUMO gap. The difference in the calculated binding energies is minor (see Table III) because in the staggered form there are also destabilizing interactions (or repulsions) between the *occupied* b_1 orbital of H_2PP ($1b_1$ in Figure 1) and some occupied b_1 levels located on the axial fluorines. On the other hand, the difference in the HOMO–LUMO gap is quite significant (see Table III) and should give the eclipsed form more kinetic stability. With a calculated binding energy of 4.9 eV (at our level of calculation we say that both isomers are energy degenerate),

we can conclude that NiF_3^+ should be a reasonable candidate to give a stable complex with R_2P-P.

$PtCl_3^+$ gives much less binding energy with a significant preference for the staggered form (see Table III). As with NiF_4^+, the b_1-b_1 bonding interaction is very weak because of both poor overlap and energy matching. This also gives a large resulting P → Pt electron migration. Although the HOMO–LUMO gap is larger than with $W(CO)_3$, $PtCl_3^+$ forms a less bound complex than the two other d^6 ML_3 fragments.

IV. Binding to C_{2v} ML_4 Fragments

The orbital pattern for a C_{2v} ML_4 fragment is "three below two". Above the three d orbitals remaining from the t_{2g} set of the octahedron stand two hybrids, b_2 and a_1 (**9**).

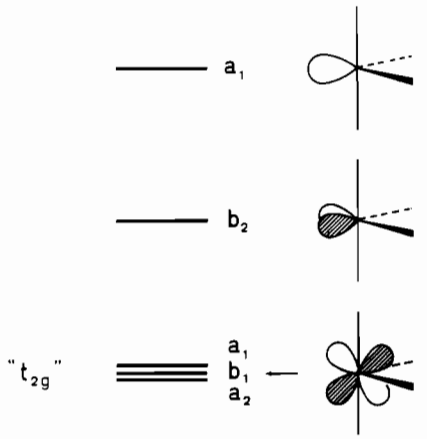

9

One immediately sees that the best bonding with H_2P-P will be obtained if both b_2 and a_1 are empty and therefore able to receive the two lone pairs from the phosphinidene end, while b_1 is occupied and can transfer electrons to the empty b_1 orbital of H_2P-P. This favorable triple-bonding scheme requires a d^6 electron count on the metal. This is accomplished for instance in $W(CO)_4$, $Cr(CO)_4$, and Mn(Cp)CO (giving **10**) and also in

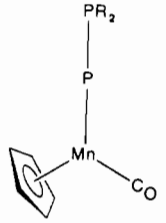

10

$Fe(CO)_4^{2+}$, $Fe(Cp)CO^+$, or $Fe(C_6H_6)CO^+$. The orbital interaction diagram between $W(CO)_4$ and H_2P-P is shown in Figure 4. Note that the equatorial ligands eclipse the PH bonds (**11a**). The other conformation in which the PH bonds eclipse the axial ligands, **11b**, is less favorable energetically (the energy difference is 1 eV with $Fe(CO)_4^{2+}$).[22]

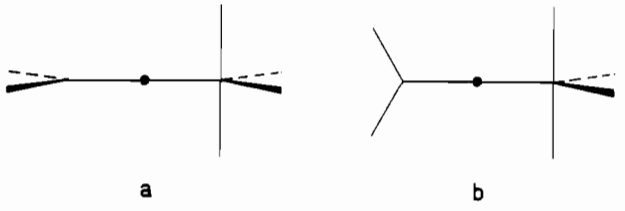

11

The binding energies and various indexes for some typical H_2PP-ML_4 complexes are given in Table II. They indicate, in most cases, strong P–M bonds. $W(CO)_4$ and Mn(Cp)CO offer the strongest binding. For $W(CO)_4$, we notice in Figure 5 a very good b_1-b_1 energy matching. This is responsible for the small overall P → W electron transfer.

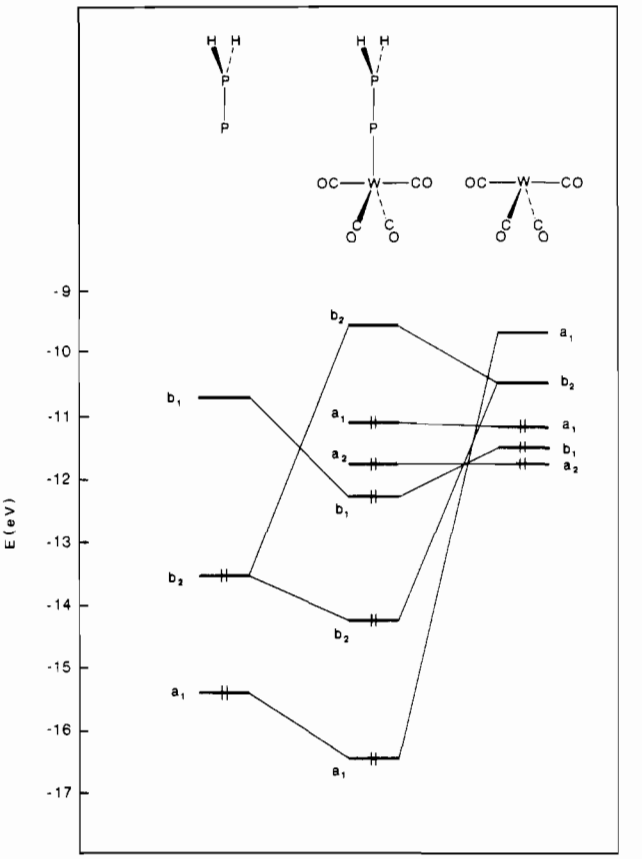

Figure 4. Interaction diagram for $H_2PP-W(CO)_4$.

$Fe(CO)_4^{2+}$ exhibits weaker binding because of the poor b_1-b_1 energy matching (−13.25 eV vs. −10.70 eV). This implies a weak b_1-b_1 bonding interaction and results in a less multiple P–Fe bond, a more multiple P–P bond, and a large P → Fe whole electron transfer (see Figure 6, right, and Table II). The Mn(Cp)CO fragment exhibits very good overlap and energy matching with H_2P-P. It gives the most strongly bound complex of the series, as all indexes in Table II are favorable.

The bonding properties of $Fe(Cp)CO^+$ and $Fe(C_6H_6)CO^{2+}$ are better than those of $Fe(CO)_4^{2+}$. In these two fragments the occupied b_1 orbital is higher than in $Fe(CO)_4^{2+}$ (−12.55 eV and −12.58 eV respectively vs. −13.25 eV) and matches better the b_1 orbital of H_2P-P (the overlap being the same in the three complexes: $\langle b_1|b_1\rangle \cong 0.13$). The b_1-b_1 mixing is now stronger, leading to increased binding energy and P–Fe overlap population and to decreased electron P → Fe transfer and P–P overlap population, as can be seen in Table II. Among other possible d^6 ML_4 fragments we also suggest $Cr(C_6H_6)CO$, giving **12**, and CrCpNO, giving **13**.

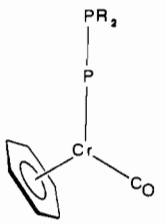

12

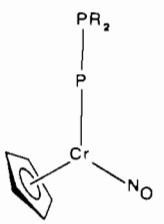

13

Recently, a stable complex of an aminonitrene with an iron(II)–tetraphenylporphyrin system (**14**) has been reported.[2d] An aminonitrene ligand is valence isoelectronic to a phosphinophosphinidene ligand. The metallic part of this complex is clearly

(22) If we consider the neutral fragment d^8 $Fe(CO)_4$, the complex is still bound (by ~1 eV) but the two forms, **11a** and **11b**, are now nearly degenerate in energy.

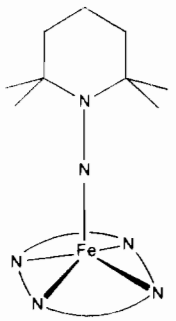

14

a d^6 ML_4 fragment. The X-ray structure of this five-coordinate square-pyramidal complex shows that the iron atom lies as far as 0.5 Å above the mean plane of the porphyrin nitrogens. The metallic part may be seen as a distorted C_{2v}-shaped ML_4 fragment. In figure 4, such as distortion should hybridize the metal b_1 orbital, increasing its interaction with the ligand b_1 orbital. Although the NR_2 group does not eclipse any Fe–N bond in **14** (possibly for steric reasons), this stable complex is in agreement with our findings.

V. Binding to C_{2v} ML_2 Fragments

Let us use again the isolobal analogy to suggest a fragment that is directly derived from d^6 ML_4. This is d^8 ML_2, which should exhibit bonding properties similar to those of d^6 ML_4 since both fragments have similar frontier orbitals (**15**).

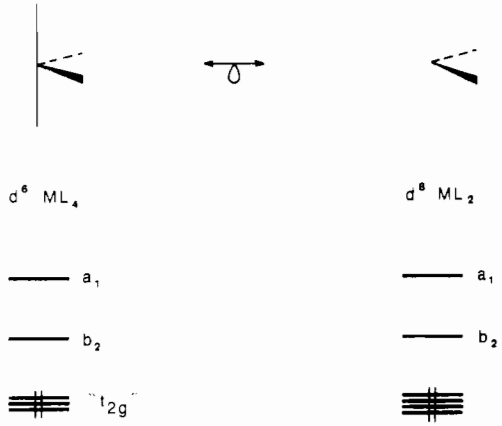

15

One can see in Figure 5 that the orbital interactions occurring in H_2PP–$Fe(CO)_2$ are quite analogous to that in H_2PP–$Fe(CO)_4^{2+}$. Note that we keep an eclipsed form for the H_2PP–ML_2 complex. The staggered form is in any case less favorable for the binding energy and again affords a narrow HOMO–LUMO gap. The values given in Table II show that the bonding capabilities of $Fe(CO)_2$ are noticeably better than those of $Fe(CO)_4^{2+}$. The HOMO–LUMO gap is reduced but still large enough to insure sufficient kinetic stability.[23]

We next studied two d^8 C_{2v} ML_2 fragments containing nickel: $Ni(CN)_2$ and $NiCl_2$.[24] It can be seen in Table II that these two fragments give weaker binding energies.

VI. Binding to C_{3v} ML_3 Fragments

Another important class of fourteen-electron metallic fragments is d^8 C_{3v} ML_3. One common representative of this class is Fe-$(CO)_3$, which can be generated easily from $Fe_2(CO)_9$ or other species.[25] An orbital interaction diagram for H_2PP–$Fe(CO)_3$ is shown in Figure 6. The whole symmetry of the complex is only C_s, so the main bonding interactions are now named a″ (b_1–e), a′ (b_2–e) and a′ (a_1–a_1).

The orbital pattern for $Fe(CO)_3$ is "three below three" (**16**).[20] The conditions of overlap and energy matching of the higher hybrids and the metal orbitals with our ligand orbitals happen to be very favorable and lead to very strong bonding interactions.

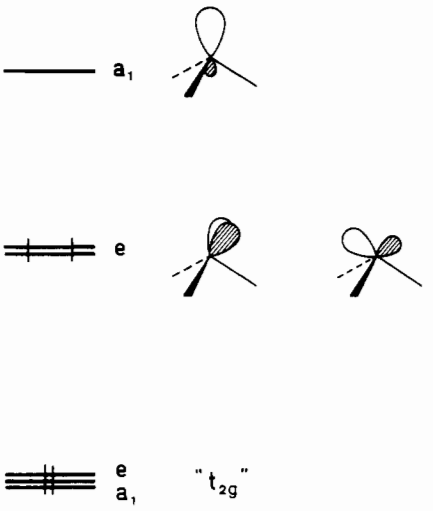

16

This results in the values given in Table II, namely (1) a large binding energy (>6 eV), (2) a large P–Fe overlap population (1.24), (3) a weak P–P overlap population and a weak resulting P ← Fe electron transfer [all of these being due to the strong a″ (b_1–e) interaction (notice in Figure 6 the very good energy matching)], and (4) a large HOMO–LUMO gap (2.5 eV). Since in $Fe(CO)_3$ the higher a′ and a″ orbitals are degenerate in an e set, besides the conformation taken in Figure 6, **17**, there is another conformation, **18**, which is virtually isoenergetic.

17 18

Obviously, $Fe(CO)_3$ should form, with R_2P–P, the most stable complex we have considered up to this point. We next considered two other iron d^8 C_{3v} ML_3 fragments, $FeCp^-$ and $Fe(\eta^6\text{-}C_6H_6)$. Our results on the two corresponding complexes, **19** and **20**, are reported in Table II. They are basically the same as those obtained with $Fe(CO)_3$.

19 20

The orbital interaction diagram for H_2PP–$FeCp^-$ is given in Figure 7, right. As expected, the orbital pattern for $FeCp^-$ is similar to that of its isolobal $Fe(CO)_3$.[26] All levels have been pushed up in energy, especially the low-lying empty a_1 orbital.

(23) It can be deduced from Figure 5 (left) that the fragment $Fe(CO)_2^{2+}$ may give a high-spin complex of about the same binding energy as H_2PP–$Fe(CO)_2$.

(24) Note that the parameters used for Ni^{II} are different from those used for Ni^{IV} (NiF_3^+, NiF_4) or Ni^{VI} (NiF_4^{2+}). This allows us to have reasonable net charges on nickel in all cases. It does not significantly change the shape of the orbital interaction diagrams nor the values listed in Table II. For $Ni(CN)_2$, when they are computed with Ni^{IV} or Ni^{VI} parameters, these values become 2.73, 0.92, 1.32, 1.04 (P → Ni), and 1.23 eV, respectively.

(25) Fleckner, H.; Grevels, F. W.; Hess, D. *J. Am. Chem. Soc.* **1984**, *106*, 2027.

(26) Albright, T. A. *Tetrahedron* **1982**, *38*, 1339.

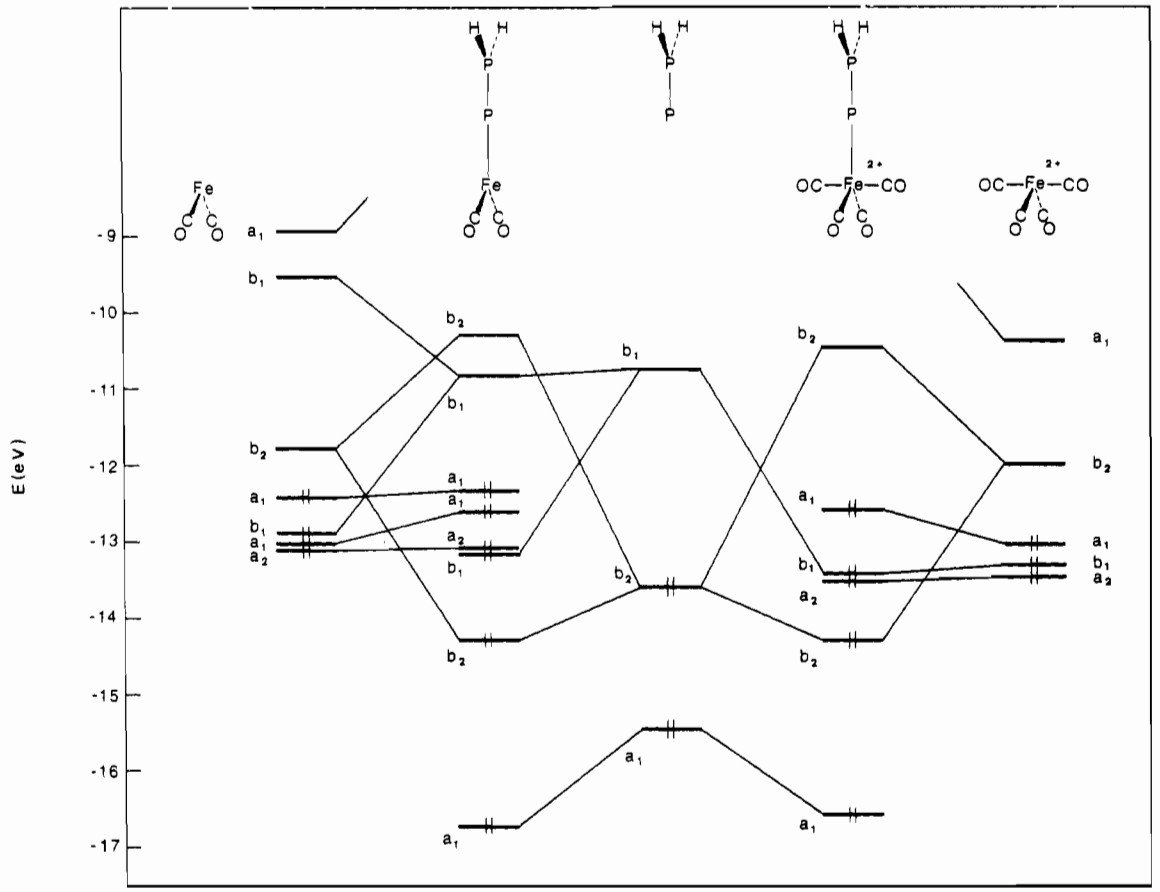

Figure 5. Interaction diagrams for $H_2PP-Fe(CO)_4^{2+}$ (right) and $H_2PP-Fe(CO)_2$ (left).

Table IV. Overlaps for Relevant Orbitals of H_2P-P and d^8 ML_3 Fragments

metallic fragments	$\langle b_1\|e_1\rangle$	$\langle b_2\|e_1\rangle$	$\langle a_1\|a_1\rangle$
$Fe(CO)_3$	0.17	0.20	0.44
$FeCp^-$	0.15	0.18	0.71
$Fe(\eta^6\text{-}C_6H_6)$	0.16	0.19	0.70
CoCp	0.09	0.10	0.68

The top half-filled e_1 level (the complex remains at C_s symmetry but the fragment $FeCp^-$ is now of C_{5v} symmetry) is now above the b_1 level of H_2P-P, affording slightly more stabilizing a'' (b_1–e_1) interaction. There is also a low-lying filled e_1 level, close to b_2 of H_2P-P, that gives a secondary interaction in the a' (b_2–e_1) mixing.

We give in Table IV the values of the overlap between the relevant orbitals of H_2P-P and d^8 ML_3 fragments. In the iron series, only the $\langle a_1|a_1\rangle$ overlap is very different when going from $Fe(CO)_3$ to $FeCp^-$ or $Fe(C_6H_6)$. In those two fragments the empty a_1 orbital is very concentrated on the metal atom: the reduced charge matrix indicates that this a_1 orbital is located at 97% on the iron atom in $FeCp^-$ and $Fe(C_6H_6)$ vs. only 44% in $Fe(CO)_3$ due to the well-known mixing with carbonyl π^* orbitals.[20] This gives a very large overlap with a_1 of H_2P-P, which actually compensates for the poor a_1–a_1 energy matching. Finally the b_1–e_1 bonding interaction makes the difference between $H_2PP-Fe(CO)_3$ and $H_2PP-FeCp^-$. This interaction is larger in the latter compound giving more binding energy, a larger resulting P ← Fe electron transfer, and a smaller P–P overlap population (see Table II).

The orbital pattern for the $Fe(C_6H_6)$ fragment[27] is almost the same as for $FeCp^-$. The only difference is that the half-filled e_1 level is pushed down in energy, now lying below the empty b_1 level of H_2P-P. This creates slightly less energy gain and P ← Fe electron transfer in the a' (b_1–e_1) interaction. This approximates the situation with $Fe(CO)_3$. Actually, as regards the calculated parameters of Table II, there is no significant difference between $Fe(CO)_3$ and $Fe(C_6H_6)$.

CoCp is a more disappointing fragment. Neither the binding energy nor the other indexes given in Table II makes it as favorable a fragment as the other d^8 ML_3 fragments we have considered in this work. The orbital interaction diagram for CoCp is given in Figure 7, left, allowing a direct comparison with its isoelectronic neighbor. Two things are common to $FeCp^-$ and CoCp. The first is the position and the nature of the empty a_1 orbital, localized at 97% on the metal. The second is the existence of an occupied e_1 level close in energy to the occupied b_2 level of H_2P-P, which comes to interfere in the a' (b_2–e_1) bonding interaction. The main difference between the two fragments is the position and the nature of the half-filled e_1 orbital. In CoCp this orbital is lower in energy, lying below the empty b_1 orbital of H_2P-P. In addition, its nature is less concentrated on the metal (only 37%) than it was in $FeCp^-$ (59%). Consequently the $\langle b_2|e_1\rangle$ and $\langle b_1|e_1\rangle$ overlaps are both weaker (by nearly half) with CoCp than with $FeCp^-$ as can be seen in Table IV. These two factors contribute to a smaller b_1–e_1 bonding interaction in $H_2PP-CoCp$. This leads to a reduced metal → phosphorus electron donation, leading in turn to an overall electron transfer in the P → Co direction together with a less weakened P–P bond and finally a decreased binding energy.

Another consequence of the poor b_2–e_1 overlap and orbital interaction is the relatively low-lying LUMO, which contributes to a narrow HOMO–LUMO gap and may eventually reduce the kinetic stability of $R_2PP-CoCp$.

VII. Binding to C_{3v} ML_4 Fragments

Another possible fragment, C_{3v} NiF_4, gives **21**. NiF_4 has a set of frontier orbitals that is very concentrated and located around −14 eV, i.e. close to the b_2 occupied orbital of H_2P-P (see Figure 8). As occurred with NiF_3^+, there is no significant bonding interaction with the empty b_1 orbital of H_2P-P. The bonding in complex **21** occurs therefore through b_2–e and a_1–a_1 interactions. This gives a significant P → Ni gross charge migration together

(27) Muetterties, E. L.; Bleeke, J. R.; Wucherer, E. J.; Albright, T. A. *Chem. Rev.* **1982**, *82*, 499.

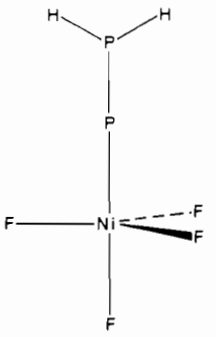

21

with a nonweakened P–P bond, as in the case of NiF_3^+ (see Table II).[28] Figure 8 also shows that nothing is changed either in the bonding or in our numerical values if we consider the fragment NiF_4^{2+}, when it gives a high-spin complex $H_2PP–NiF_4^{2+}$. Finally, NiF_4 is a candidate that furnishes more binding energy than d^8 NiL_2 but less than NiF_3^+. The general type d^6 C_{3v} ML_4 can be considered as a favorable fragment for bonding to our model ligand, keeping in mind that changing the nature of the ML_4 atoms should afford more b_1–b_1 type mixing by raising the metal orbitals.

VIII. η^2 Binding

We have seen that $H_2P–P$ has an occupied π MO and an empty π^* MO. This orbital similarity to ethylene leads us to think about the possibility of $H_2P–P$ as a side-on ligand, as C_2H_4 is in Zeise's complex (**22**).[29] We have thus studied its analogue (**23**). The

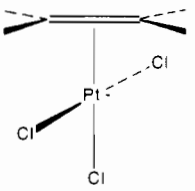

22

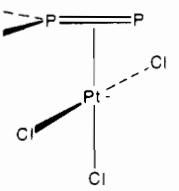

23

corresponding orbital interaction diagram is given in Figure 9. The two orbitals of $H_2P–P$ that are involved in bonding interactions are now occupied $1b_1$ π_{PP} and empty $2b_1$ π^*_{PP}. The symmetry of the whole complex is only C_s, allowing orbital mixings, but the main interactions are clearly visible in Figure 10. The main bonding interaction is by far that which involves the empty π^*_{PP} orbital, which overlaps well with the occupied orbital at the bottom of the "t_{2g}" set of $PtCl_3^-$. The interaction involving occupied π_{PP} is less energy gaining, partly due to a secondary interaction with a lower occupied orbital of $PtCl_3^-$. The a_1 lone pair of $H_2P–P$ still has the right symmetry to delocalize into the empty a_1 orbital of $PtCl_3^-$, giving a significant stabilizing interaction. The b_2 lone pair of $H_2P–P$ encounters only occupied orbitals of the same symmetry (a″) in $PtCl_3^-$. This will give a destabilizing interaction. Finally, the binding energy is very weak, and both Pt–P overlap populations are weak (see Table I). As expected from the predominant π^*–d mixing, the P–P bond is much weakened and the resulting electron transfer is in the P ← Pt direction.

Note that in Zeise's salt the π and π^* levels of ethylene are both higher in energy (−13.3 and −8.0 eV, respectively), allowing a stronger π_{CC}–a_1 bonding interaction while the π^*_{CC}–b_1 bonding interaction should be weaker. The last point is generally compensated by a cis bending of the olefin substituents away from the metal. This results in a lowering of the π^* level and an increase

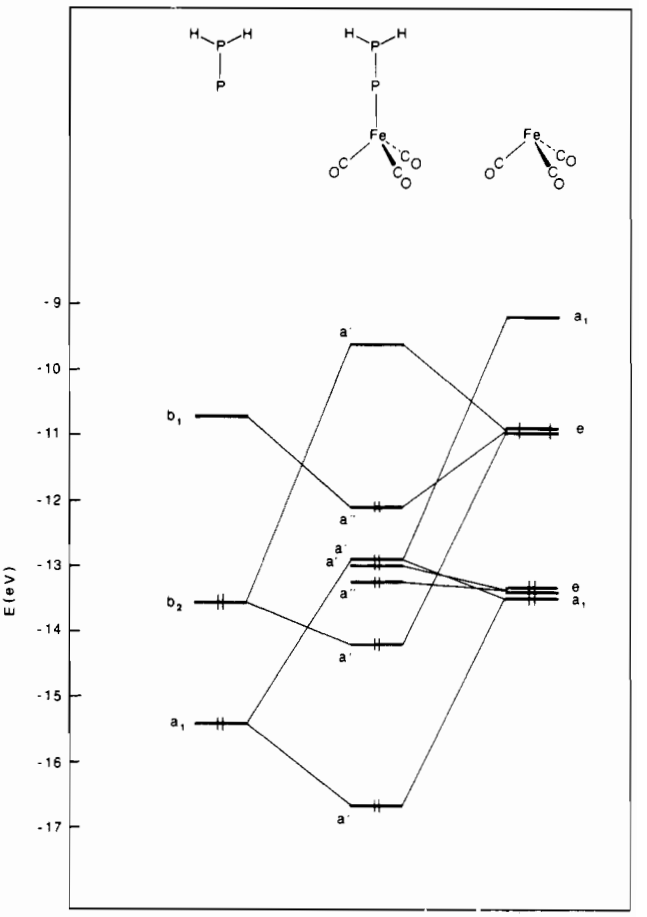

Figure 6. Interaction diagram for $H_2PP–Fe(CO)_3$.

of its overlap with the metal b_1 orbital.[29a] Such a puckering of the hydrogens in our case (i.e. a pyramidalization of PH_2) may also be expected to strengthen the bonding by improving the b_1–b_1 interaction.

The σ lone pair on the terminal phosphorus is not closely involved in the bonding and remains available for coordinating another metal, giving a dinuclear complex (**24**). Since this orbital

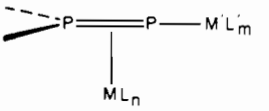

24

is low in energy (−15.8 eV; see Figure 9), the $M'L'_m$ group should have a low a_1-type acceptor orbital. This might be realized for instance with AuR^+.[30]

If we tilt $H_2P–P$ to obtain the eclipsed form of the η^1 complex (**25**), the strength of the binding is not dramatically changed (see Table I); 0.3 eV has been gained in energy. The two bonding interactions are now a_1–a_1 and b_1–b_1; an orbital interaction diagram shows that the b_2–b_2 interaction is still very repulsive through a three-orbital six-electron interaction.

The staggered form of the η^1 complex (**26**) turns out to be more stable. The orbital interaction diagram shows a less strong b_1–b_1 bonding interaction. There is, at the same time, a less repuslive b_2–b_2 interaction (involving only two orbitals and four electrons), the a_1–a_1 interaction remaining the same. This results in stronger binding, as can be seen in Table I. In summary, with $PtCl_3^-$, $R_2P–P$ forms a η^1 staggered complex, rather than a η^2 complex. This η^1 complex however is much more stable when the $PtCl_3$ fragment has a d^6 electron count (i.e. PCl_3^+) as was discussed previously.

(28) Actually, the P–P overlap population in both $H_2P–P–NiF_3^+$ and $H_2P–P–NiF_4$ is calculated at 1.35, which is above the value for isolated $H_2P–P$ (1.34). This is due to the fact that in these complexes we have not *populated* the b_1 MO of $H_2P–P$, which is P–P *antibonding*, while we have *depopulated* the b_2 MO, which is slightly P–P *antibonding*.

(29) For MO treatments of transition-metal-complexed olefins, see: (a) Albright, T. A.; Hoffmann, R.; Thibeault, J. C.; Thorn, D. L. *J. Am. Chem. Soc.* **1979**, *101*, 3801. (b) Eisenstein, O.; Hoffmann, R. *J. Am. Chem. Soc.* **1981**, *103*, 4308. (c) Hoffmann, R. *Science (Washington, D.C.)* **1981**, *211*, 995.

(30) Komiya, S.; Albright, T. A.; Hoffmann, R.; Kochi, J. K. *J. Am. Chem. Soc.* **1976**, *98*, 7255.

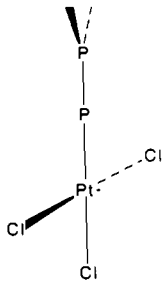

25

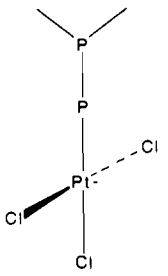

26

IX. $(H_2N)_2P$–P Ligand

In the same way that a π conjugation stabilizes H_2P–P with respect to H–P, any further substitution of hydrogen by a π-donor group, such as an amino group, should intrinsically stabilize the >P–P framework or any valence isoelectronic analogues such as >N–P, >P–N, or >N–N. Does this enhanced conjugation strengthen or weaken the bonding of R_2P-P to a metal fragment? Figure 10 displays what is changed in the MO pattern of H_2P–P when the hydrogens are replaced by amino groups to give planar $(H_2N)_2P$–P. The occupied a_1 and b_2 orbitals, which correspond to the two lone pairs of the phosphinidene end, have not been dramatically modified either in energy or in shape. The π orbitals now form a trimethylenemethane-like set. $1b_1$, the in-phase combination of p atomic orbitals, has been pushed down in energy, but this is without important consequences for the bonding. The empty π^* orbital, $3b_1$, which is important for the bonding, has been pushed up in energy by more than 2 eV[31] while its nature is inevitably less localized on the terminal phosphorus. Both effects are enough to reduce the b_1–b_1 bonding interaction in a complex, through poor energy matching and smaller b_1–b_1 overlap. But there is more. In the π set of $(H_2N)_2P$–P, there are two high-lying occupied orbitals. a_2 is mainly localized on the N_2P– end and should not interfere in the bonding. On the other hand $2b_1$ has a large coefficient on the terminal phosphorus and should weaken the bonding through mixing in the b_1–b_1 bonding interaction or through repulsive interaction with an eventual occupied b_1 orbital of the metallic fragment.

The orbital interaction diagram for $(H_2N)_2PP$–$W(CO)_4$ is shown in Figure 11. Let us compare it with the same diagram for H_2PP–$W(CO)_4$ (Figure 4). The a_1–a_1 bonding interaction is less stabilizing. This may be ascribed to a weaker $\langle a_1|a_1\rangle$ overlap. As expected from the identical b_2 orbitals in H_2P–P and $(H_2N)_2P$–P, the b_2–b_2 bonding interactions are nearly identical in the two complexes. Much is changed in the b_1–b_1 interaction. With H_2P–P (Figure 4) we had a clear-cut two-orbital interaction whereas with $(H_2N)_2P$–P (Figure 11) we have a four-orbital six-electron interaction that does not bring any energy benefit. The calculated indexes listed in Table V all indicate less strong binding of $(H_2N)_2P$–P. The binding energy has dropped to 2.9 eV (vs. 5.1 eV for H_2P–P); the P–W total overlap population has dropped to 1.1 (vs. 1.2 for H_2P–P). As expected from the poor involvement of the empty b_1 orbital in the bonding, the resulting P → W electron transfer is enhanced (0.52 vs. 0.17) and the P–P overlap population is not reduced with respect to its value in the isolated molecule (1.20).

A similar analysis can be performed for the complex $(H_2N)_2P$–P–$Fe(CO)_3$. The calculated values given in Table V also indicate that the strength of the P–Fe link is largely reduced in the diamino complex. Note that this time, the decrease of empty b_1 orbital involvement in the bonding helps to reverse the direction of the whole electron transfer. For this complex we give in Table VI the values of the overlap for the three couples of relevant orbitals. This illustrates what we said above on the nature of some orbitals in $(H_2N)_2P$–P.

The last comment we shall make on all these numerical values concerns the HOMO–LUMO gaps. In the complexes with $W(CO)_4$, the HOMO–LUMO gap is virtually the same if the ligand is H_2P–P or $(H_2N)_2P$–P. Figures 4 and 11 are self-explanatory for this. On the other hand, Figure 6 makes clear why the HOMO–LUMO gap in the complexes with $Fe(CO)_3$ varies with the amount of the b_1–b_1 bonding interaction. Actually, this gap is reduced by half if the ligand is $(H_2N)_2P$–P instead of H_2P–P. This is due to a poor b_1–e interaction, inducing a higher a″ HOMO level.

By analogy with trimethylenemethane, a π complexation (i.e. η^4 binding) can be considered for our ligand. Trimethylenemethane has four π electrons and binds typical d^8 ML_3 fragments such as $Fe(CO)_3$.[32] $(H_2N)_2PP$ has six π electrons and therefore may be expected to bind d^6 ML_3 fragments (**27**). Three examples

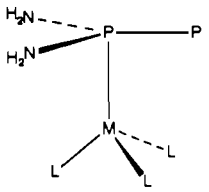

27

have been studied here: $W(CO)_3$, $Fe(CO)_3^{2+}$, and $Ni(CO)_3^{4+}$. The results are reported in Table V. The calculated binding energies are weak in any case, suggesting that this mode of binding is not favorable for our ligand. The interaction diagrams show that the bonding interactions (b_1–a_1 and b_1,a_2–e) remain weak even when the energy match is favorable such as with $Ni(CO)_3^{4+}$. The main reason for the weak interactions is the poor overlap between the relevant orbitals. Although bringing the planar ligand closer to the metal (for metal to central phosphorus distances shorter than 2 Å) does not improve the bonding (the binding energy is reduced), a puckering of the ligand, as observed in the trimethylenemethane complexes, should greatly strengthen the bonding.

We have just shown that the binding of a phosphino-phosphinidene to a transition-metal fragment is less strong when the phosphino part bears π-donor substituents such as amino groups. At this point an important remark must be made. In searching for potentially viable R_2PP–MLn complexes, one must keep in mind that the R_2P–P part must possess a certain intrinsic stability, otherwise the stabilization brought by the metal complexation may not be sufficient to trap it in its phosphino-phosphinidene form. Since this essential requirement can be met by using π-donor substituents, it is reasonable to think that $(R_2N)_2P$–P ligands should form metallic complexes that are more viable than the ones formed from simple R_2P–P ligands.

X. H_2N–P, H_2N–N, and H_2P–N Ligands

Let us consider now some singlet species that are valence isoelectronic with H_2P–P and in which one or two phosphorus atoms are substituted by nitrogen. These are H_2N–P, H_2N–N, and H_2P–N. The relevant energy levels for these species are shown in Figure 12. Some pertinent overlaps with the $Fe(CO)_3$ fragment are listed in Table VI, and the numerical results for the corresponding complexes are reported in Table V.

Aminophosphinidene. The $\langle b_1|e\rangle$ and $\langle a_1|a_1\rangle$ overlaps are slightly smaller than in phosphinophosphinidene. On the other hand, the empty b_1 level is significantly lower in energy, which should give, in the complex with $Fe(CO)_3$, (1) an increased binding energy and (2) an increased P ← Fe electron migration through b_1–b_1 mixing. This appears in the calculated values listed in Table V. To sum up, we can say, however, that both phosphino- and aminophosphinidene exhibit comparable properties for bonding to $Fe(CO)_3$.

Aminonitrene. Table VI shows that all overlaps are much weaker. The energy levels of H_2N–N are close to those of H_2P–P, except the HOMO, b_2 orbital, which is higher and should afford

(31) The resulting increase of the HOMO–LUMO gap is, in our approach, what favors a closed-shell singlet ground state in $(R_2N)_2P$–P.

(32) Albright, T. A.; Hofmann, P.; Hoffmann, R. *J. Am. Chem. Soc.* **1977**, *99*, 7546.

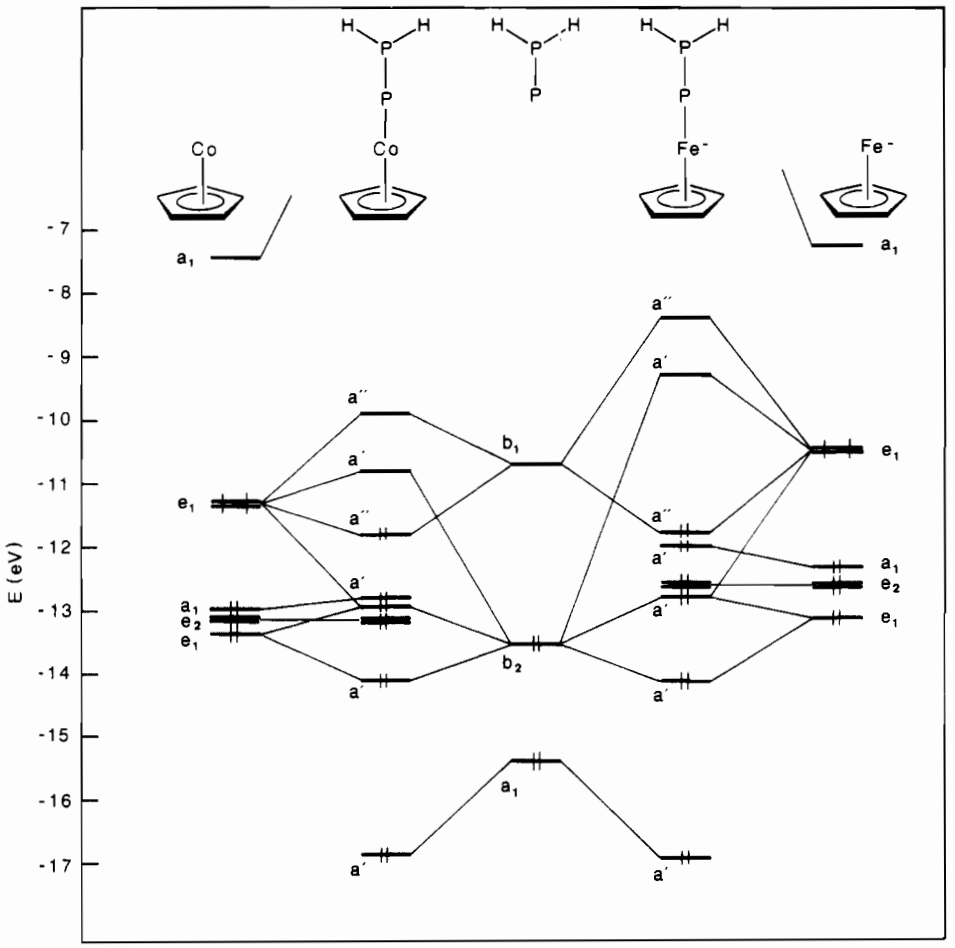

Figure 7. Interaction diagrams for $H_2PP-FeCp^-$ (right) and $H_2PP-CoCp$ (left).

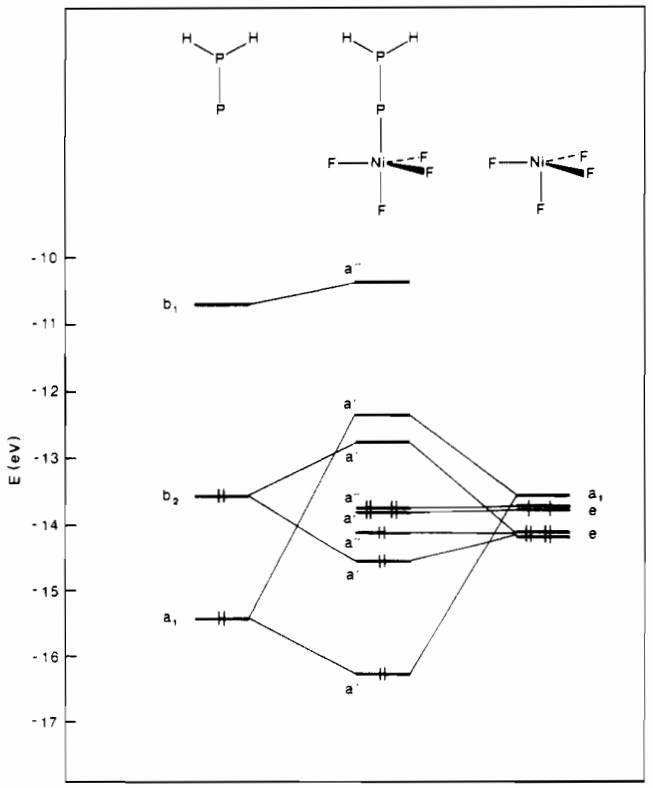

Figure 8. Interaction diagram for $H_2PP-NiF_4$.

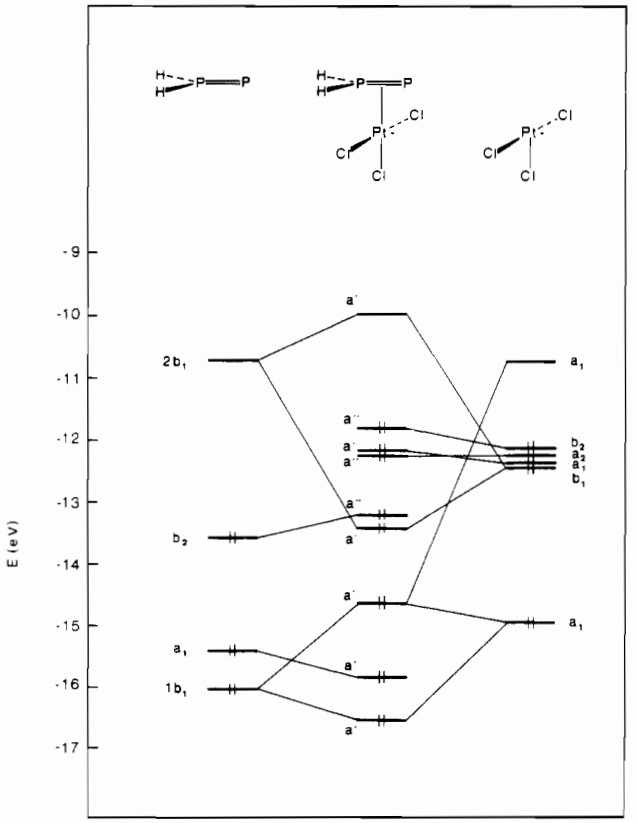

Figure 9. Interaction diagram for η^2-$H_2PP-PtCl_3^-$.

a better energy match. Poor overlaps prevail in making all bonding interactions weaker. The complex $H_2NN-Fe(CO)_3$ is therefore bound much less than the complex $H_2PP-Fe(CO)_3$ as indicated by the calculated binding energy and other indexes listed in Table V.

Table V. Main Results for Complexes Involving Various R_nX–Y Ligands

ligands	metallic fragments	ΔE, eV	tot. overlap pop. Y–M	tot. overlap pop. X–Y	tot. overlap pop. X–Y in ixolated ligand	gross charge transfer, e Y → M	gross charge transfer, e Y ← M	Δ(HOMO–LUMO), eV
$(H_2N)_2P$–P	$W(CO)_4$	2.91	1.08	1.21	1.20	0.52		1.42
$(H_2N)_2P$–P	$Fe(CO)_3$	3.79	1.12	1.16	1.20	0.43		1.10
η^4-$(H_2N)_2P$–P	$W(CO)_3$	1.47	0.28[a]	0.14[a]	0.07[a]	0.22		1.38
η^4-$(H_2N)_2P$–P	$Fe(CO)_3^{2+}$	1.28	0.28	0.11	0.06	0.49		2.47
η^4-$(H_2N)_2P$–P	$Ni(CO)_3^{4+}$	1.16	0.29	0.10	0.05	0.83		1.34
H_2P–P	$Fe(CO)_3$	6.12	1.24	1.05	1.34		0.02	2.48
H_2N–P	$Fe(CO)_3$	6.81	1.24	0.78	1.00		0.20	2.89
H_2N–N	$Fe(CO)_3$	4.49	0.95	0.92	1.16		0.05	1.60
H_2P–N	$Fe(CO)_3$	4.45	0.93	0.91	1.18		0.27	1.57
H_3C–P	$Fe(CO)_3$	9.51	1.24	0.75	0.87		0.45	3.48
H_5C_6–P	$Fe(CO)_3$	7.46	1.23	0.84	0.94		0.41	2.75

[a] For for the η^4 π complexes the three reported total overlap populations correspond to the three kinds of bonds: P(central)–M, P(terminal)–M, and N–M, respectively.

Table VI. Overlaps for the Relevant Orbitals of $Fe(CO)_3$ and Various Phosphinidene or Nitrene Ligands

ligands	$\langle b_1\|e\rangle$	$\langle b_2\|e\rangle$	$\langle a_1\|a_1\rangle$
$(H_2N)_2P$–P	0.12	0.20	0.39
H_2P–P	0.17	0.20	0.44
H_2N–P	0.15	0.20	0.38
H_2N–N	0.11	0.14	0.27
H_2P–N	0.11	0.14	0.28
H_3C–P	0.20	0.20	0.39

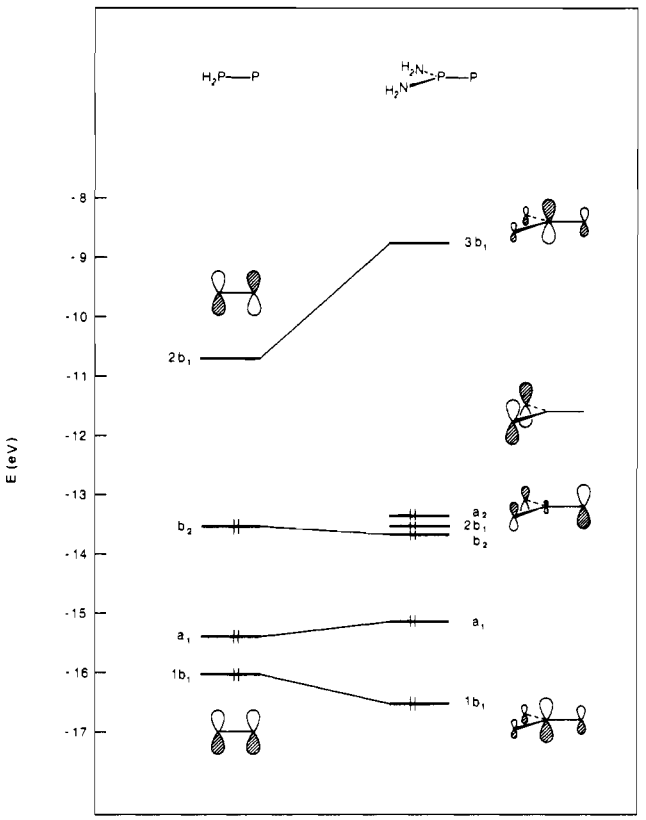

Figure 10. Main molecular orbitals of (diaminophosphino)phosphinidene as derived from phosphinophosphinidene. Only the shapes of the π orbitals are plotted.

Phosphinonitrene. The binding of phosphinonitrene H_2P–N to $Fe(CO)_3$ presents characteristics similar to the binding of aminonitrene, generalizing that the nitrene complexes are less bound than the phosphinidene complexes.

XI. CH_3–P and C_6H_5–P Ligands

How is the situation different when the phosphinidene does not have a π-donor group in the α position? Methylphosphinidene H_3C–P is the simplest alkyl representative for this kind of compound. Its energy levels are depicted in Figure 13, left. The two p orbitals of phosphorus are now degenerate in energy, and we should put the two last electrons in these two orbitals with their spins parallel, according to Hund's rules, thus implying a triplet open-shell ground state. Note that the two nonbonding electron pairs are both higher in energy in H_3C–P than in H_2P–P.

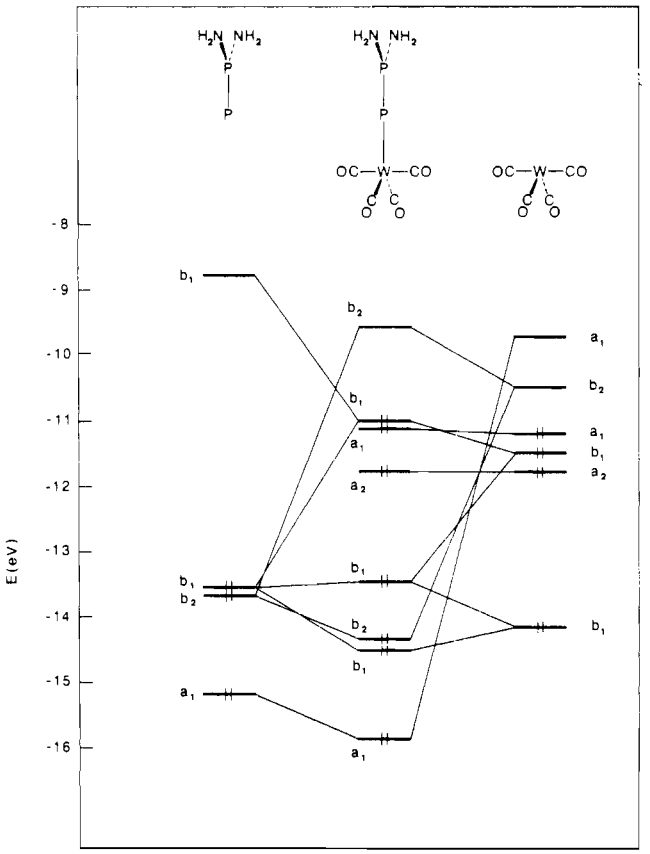

Figure 11. Interaction diagram for $(H_2N)_2PP$–$W(CO)_4$.

An interaction diagram for the H_3CP–$Fe(CO)_3$ complex is given in Figure 13. The complex has C_{3v} symmetry with free rotation around the C–P or P–Fe bond. The overlap of the relevant orbitals of the two fragments is very good as can be seen in Table VI. The energy of the half-filled degenerate level in H_3C–P is more than 2 eV below the half-filled degenerate level in $Fe(CO)_3$. All conditions are met to give a very strong bonding interaction, with a large transfer from iron to phosphorus. Actually, the results of the calculations, given in Table V, show a very large binding energy, an important P–Fe overlap population, a large HOMO–LUMO gap, and a large P ← Fe electron transfer. Although the large calculated binding energy must not be taken too literally, keeping in mind that R–P is intrinsically less stable than R_2P–P, one can conclude that alkylphosphinidenes could form terminally

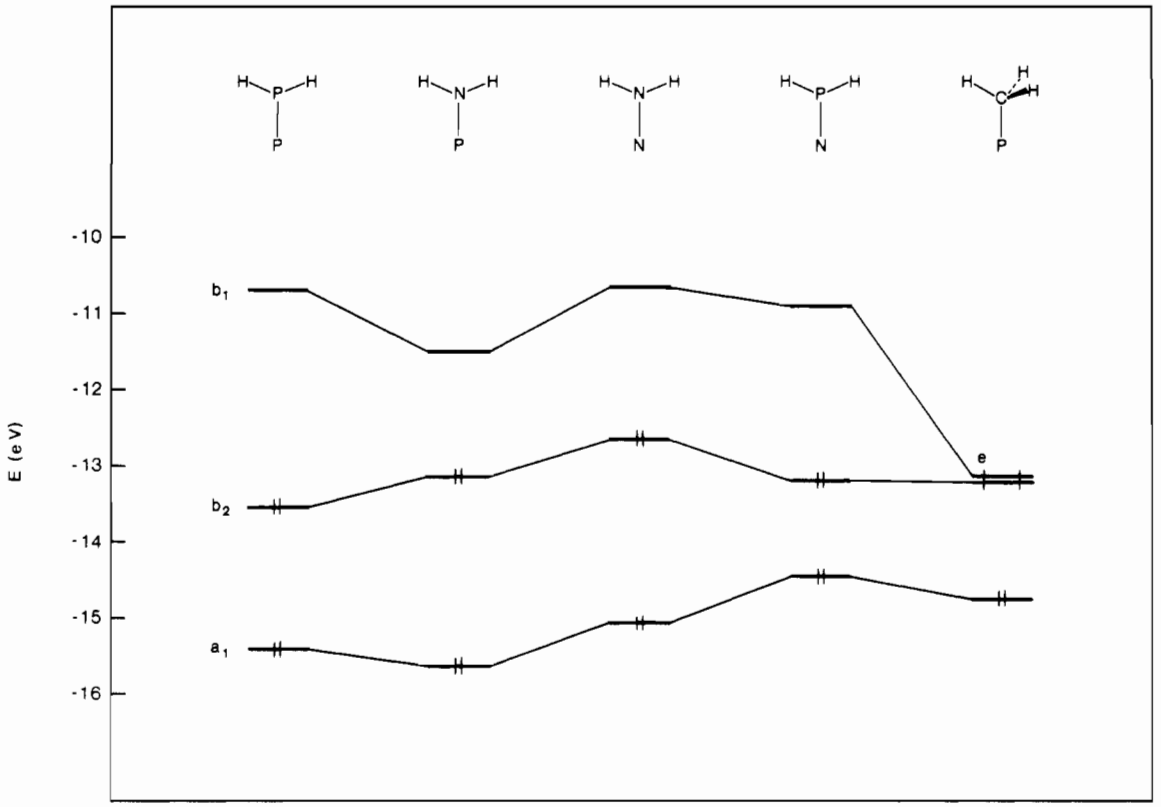

Figure 12. Energy levels in some phosphinidenes and nitrenes.

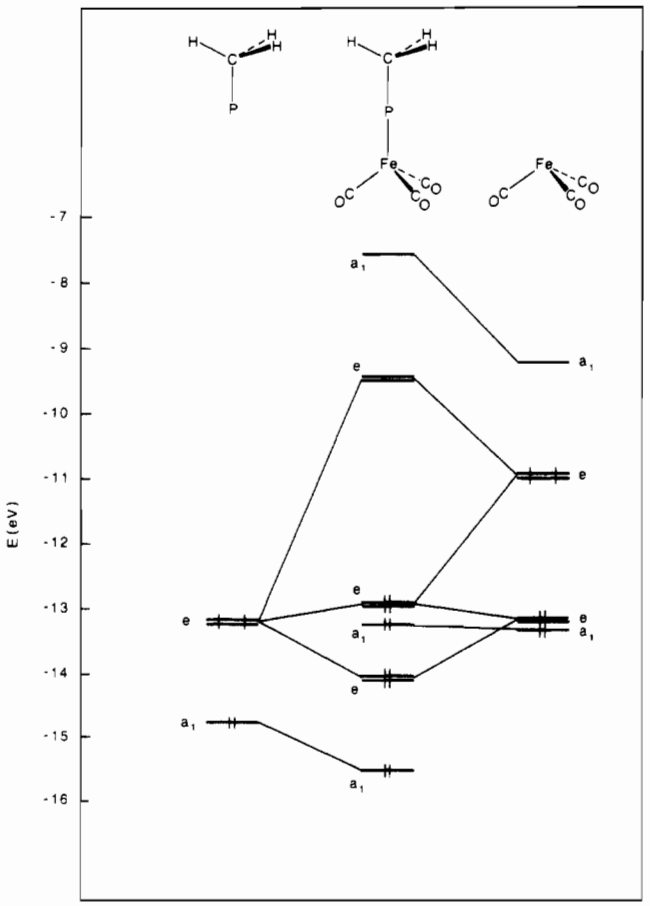

Figure 13. Interaction diagram for H_3CP–$Fe(CO)_3$.

bound end-on complexes with metallic fragments such as $Fe(CO)_3$.

Phenylphosphinidene is not a model ligand but a real phosphinidene known to give mainly bridged stable complexes. A simplified interaction diagram for PhP–$Fe(CO)_3$ is given in Figure 14. The empty b_1 orbital of Ph–P is still low in energy, favoring a large binding energy in the complex and a significant P ← Fe electron transfer. The results of Table II confirm this and show that Ph–P gives, with $Fe(CO)_3$, a complex that is between H_2P–P–$Fe(CO)_3$ and H_3CP–$Fe(CO)_3$ in strength. In reality, the large number of high-lying levels in the Ph–P ligand and the low symmetry of the complex lead to much mixing and secondary interactions, which make the FMO analysis more complicated.

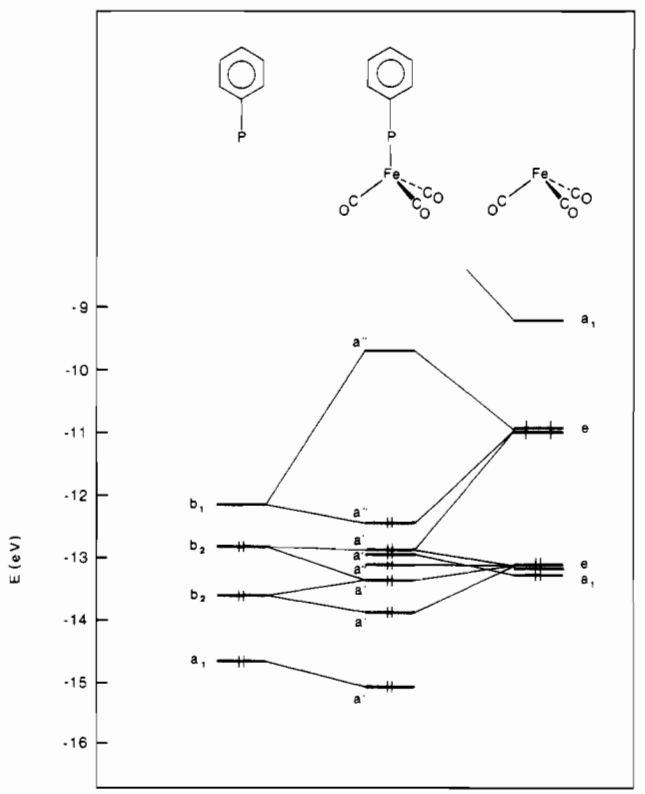

Figure 14. Interaction diagram for PhP–$Fe(CO)_3$.

Table VII. Results on Mononuclear and μ_2 Dinuclear Complexes of H_2P–P with ML_5 Fragments

fragments	ΔE, eV	tot. overlap pop. P–M	tot. overlap pop. P–P	gross charge transfer, e P → M	gross charge transfer, e P ← M	Δ(HOMO–LUMO), eV
MnH_5^{2-} d^4	5.00	1.22	1.13	0.46		1.63
MnH_5^{4-} d^6	1.74	0.83	1.16		0.16	1.42
μ_2 $(MnH_5^{4-})_2$ d^6	4.43	0.74	1.12	0.35		2.68
WH_5^{3-} d^4	6.02	1.29	1.02		0.14	1.57
WH_5^{5-} d_6	2.88	0.89	1.06		0.56	1.06
μ_2 $(WH_5^{5-})_2$ d^6	5.35	0.78	1.02		0.12	2.25

XII. Bridging in Dinuclear Systems

Bridging has been examined in the simplest case, namely μ_2 complexes. The X-ray structure of μ-PhP$[Mn(CO)_2Cp]_2$ being known,[33] we have performed calculations on model d^6 ML_5 complexes using this experimental MPM angle and M–P distance. We studied the species $H_2PP(MnH_5^{4-})_2$ and $H_2PP(WH_5^{5-})_2$ and compared the results with the mononuclear d^4 and d^6 ML_5 complexes. The numerical results are listed in Table VII. Three bonding interactions take place in the dinuclear μ_2 complexes: (1) the mixing of the occupied a_1 and b_2 orbitals of H_2PP with the in-phase and out-of-phase combinations, respectively, of the empty a_1 hybrids on ML_5 (**28**, **29**); (2) the mixing of the empty b_1 orbital

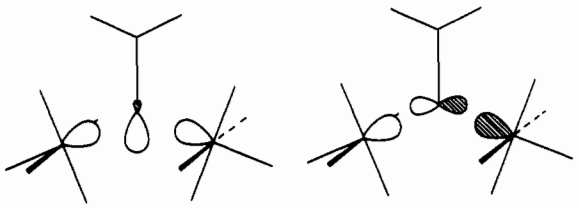

28 **29**

of H_2PP with the in-phase combination of an occupied d_π metal orbital (**30**). The interaction diagrams show that all these sta-

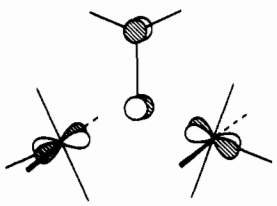

30

bilizing interactions are strong. This is mainly due to large overlaps. Actually, in $H_2PP(WH_5^{5-})_2$, the $\langle a_1|a_1\rangle$ and $\langle b_2|b_2\rangle$ overlaps happen to have their optimal value near the chosen M–P distance (2.2 Å) whereas for shorter W–P distances, the binding energy decreases. The interaction diagram for $H_2PP(WH_5^{5-})_2$ shows that the b_1–b_1 interaction is predominant here due to a good energy match. This accounts for the resulting electron transfer in the W → P direction (see Table VII).

As expected, the binding energies are larger in d^6 dinuclear μ_2 complexes than in d^6 mononuclear terminally bound complexes. The most significant and interesting result is that the μ_2 dinuclear compounds with d^6 ML_5 have about the same stabilities as the terminally bound mononuclear compounds with d^4 ML_5, although the former have larger HOMO–LUMO gaps. Therefore, if d^6 ML_5 fragments are generated in a medium containing no other oxidizing agent, the bridging mode of binding should be adopted, but if d^4 ML_5 fragments are generated, a mononuclear terminal complex of comparable stability can be expected. This should also hold for all the other favorable fragments.

In conclusion, it has been shown in this work that phosphinidenes can form stable terminal complexes: possible fragments such as d^6 ML_4 and d^8 ML_3 (e.g. $Fe(CO)_3$) have been suggested. Our qualitative and quantitative results indicate that, for the right electron count, nonbridging phosphinidene complexes should be of sufficient stability to be as viable as the known bridged polynuclear systems.

Table VIII. Extended Hückel Parameters

orbital		H_{ii}, eV	ζ_1	ζ_2	C_1[a]	C_2[a]
V	4s	−8.81	1.30			
	4p	−5.52	0.875			
	3d	−11.00	4.75	1.70	0.4755	0.7052
Cr	4s	−8.66	1.70			
	4p	−5.24	1.70			
	3d	−11.20	4.95	1.60	0.4876	0.7205
W	6s	−8.26	2.341			
	6p	−5.17	2.309			
	5d	−10.37	4.982	2.068	0.66854	0.54243
Mn	4s	−9.75	1.80			
	4p	−5.89	1.80			
	3d	−11.67	5.15	1.70	0.5139	0.6929
Fe	4s	−9.17	1.90			
	4p	−5.37	1.90			
	3d	−12.70	5.35	1.80	0.5366	0.6678
Co	4s	−9.21	2.00			
	4p	−5.29	2.00			
	3d	−13.18	5.55	2.10	0.5679	0.6059
Ni(II)	4s	−6.86	2.10			
	4p	−4.90	2.10			
	3d	−12.99	5.49	2.00	0.5634	0.6210
Ni(IV,VI)	4s	−10.95	2.10			
	4p	−6.27	2.10			
	3d	−14.20	5.75	2.30	0.5798	0.5782
Pt	6s	−9.077	2.554			
	6p	−5.475	2.535			
	5d	−12.59	6.013	2.696	0.6334	0.5513
H	1s	−13.60	1.30			
C	2s	−21.40	1.625			
	2p	−11.40	1.625			
N	2s	−26.00	1.95			
	2p	−13.40	1.95			
O	2s	−32.30	2.275			
	2p	−14.80	2.275			
F	2s	−40.00	2.425			
	2p	−18.10	2.425			
P	3s	−18.60	1.60			
	3p	−14.00	1.60			
Cl	3s	−30.00	2.033			
	3p	−15.00	2.033			

[a] Contraction coefficients used in the double-ζ expansion.

Appendix

All calculations were performed by using the extended Hückel method[34] with weighted H_{ij}'s. The values for the H_{ii}'s and orbital exponents are listed in Table VIII.

Idealized geometries were considered for all complexes. Bond lengths, as reasonable as possible, were chosen from experimental geometries of parent species[35] or, for the ligand parts, from ab initio calculations when available. The following geometrical parameters (in Å and deg) were used.

Ligands. H_2PP: P–P = 1.93, P–H = 1.40, ∠HPH = 104. $(H_2N)_2PP$: P–P = 1.93, P–N = 1.68, N–H = 1.01, all bond angles = 120. H_2NP: N–P = 1.65, N–H = 1.02, ∠HNH = 112. H_2NN: N–N = 1.23, N–H = 1.02, ∠HNH = 114. H_2PN: P–N = 1.53, P–H = 1.40, ∠HPH = 108. H_3CP: C–P = 1.85, C–H = 1.09,

(33) Huttner, G.; Müller, H.-D.; Frank, A.; Lorenz, H. *Angew. Chem., Int. Ed. Engl.* **1975**, *14*, 705.

(34) Hoffmann, R. *J. Chem. Phys.* **1963**, *39*, 1397.

(35) Some bond lengths were taken from: Wells, A. F. "Structural Inorganic Chemistry", 4th ed.; Clarendon Press: Oxford, England, 1975.

all bond angles = 109.47. C_6H_5P: C-P = 1.83, C-C = 1.40, C-H = 1.08, all bond angles = 120.

Metal Fragments. For C_{4v} ML_5 and C_{2v} ML_3, all the valence angles at the metal are equal to 90°. This gives, for V(Cp)$(CO)_2$, ∠Cp(centroid)VC(O) = CpVP(PH_2) = 125.26°. For C_{2v} ML_4 and $C_{2v}ML_2$, the valence angle at the metal between equatorial ligands is 120°. Again CpMC(O) = 125.26°. For C_{3v} ML_3, all valence angles at the metal = 90°. Bond lengths (Å): W-H = 1.80, W-C(O) = 2.06, V-Cp(centroid) = 1.95, V-C(O) = 1.90, Ni-F = 1.99, Pt-Cl = 2.30, Cr-C(O) = 1.92, Fe-C(O) = 1.80, Mn-C(O) = 1.80, Mn-Cp = 1.80, Fe-Cp = 1.70, Fe-C_6H_6-(centroid) = 1.55, Co-Cp = 1.80, Ni-C(N) = 1.90, Ni-Cl = 2.32, (W)C-O = 1.15, (V)C-O = 1.15, (Cr)C-O = 1.17, (Fe)C-O = 1.15, (Mn)C-O = 1.15, Mn-H = 1.60, W-Cl = 2.30, Ni-C(O) = 1.83, (Ni)C-O = 1.15, (Ni)C-N = 1.15. In Cp and C_6H_6 bond distances (Å) are C-C = 1.42 and C-H = 1.08.

The metal-phosphinidene distance was fixed at 2.00 Å in all η^1 complexes. In the η^2 complex H_2PP-$PtCl_3^-$, the distance between the center of the P-P bond and the metal was fixed at 2.00 Å, corresponding to a Pt-P distance of 2.3 Å. The metal-nitrene distance was fixed at 1.80 Å. In the η^4 complexes the distance between the central phosphorus and the metal was fixed at 2.00 Å. In the μ_2 complexes, the metal-phosphinidene distance was fixed at 2.20 Å and the MPM angle was fixed at 138°.

Contribution from the Departments of Chemistry, Cornell University, Ithaca, New York 14853, and University of St. Andrews, St. Andrews, Fife K716 9ST, Scotland, U.K.

Bonding in Nitrosylated Iron-Sulfur Clusters

SHEN-SHU SUNG,† CHRISTOPHER GLIDEWELL,*‡ ANTHONY R. BUTLER,‡ and ROALD HOFFMANN*†

Received August 6, 1984

The electronic structure of several binuclear and tetranuclear Fe clusters with bridging S or SH units and terminal nitrosyl ligands is analyzed. The computations point to the antibonding nature of the lowest unoccupied orbitals of these molecules, indicative of potential disruption of the clusters on reduction.

The known nitrosylated iron-sulfur cluster molecules and ions[1-4] $Fe_4S_4(NO)_4$, $[Fe_4S_3(NO)_7]^-$, $[Fe_2S_2(NO)_4]^{2-}$, and $Fe_2(SR)_2(NO)_4$ are closely related to each other chemically, as shown by the transformations[1,3,5,6]

$$Fe_2(SR)_2(NO)_4 \xleftarrow{RX} [Fe_2S_2(NO)_4]^{2-} \underset{OH^-}{\overset{H^+}{\rightleftharpoons}}$$

$$[Fe_4S_3(NO)_7]^- \underset{Na/Hg}{\overset{S_8}{\rightleftharpoons}} Fe_4S_4(NO)_4$$

Although these species are all diamagnetic in the solid state and in weak-donor solvents, in powerful donor solvents they all readily yield paramagnetic species containing a single iron atom.[7] The reduction of $Fe_4S_4(NO)_4$ yields, initially, the anion $[Fe_4S_4(NO)_4]^-$, which is subsequently converted into $[Fe_4S_3(NO)_7]^-$ along with uncharacterized byproducts. This reductive transformation is effected[2] in a solvent, THF/acetone, in which dissociation to mononuclear intermediates may occur, and it seems at least possible that both the conversion of $Fe_4S_4(NO)_4$ to $[Fe_4S_3(NO)_7]^-$ and the reverse of this may occur via a mechanism of extensive fragmentation and reassembly. The observation that $Fe_4S_4(NO)_4$ and $[Fe_4S_3(NO)_7]^-$ can both be synthesized by spontaneous self-assembly from mononuclear starting materials lends plausibility to this suggestion. Fragmentation must obviously occur in the conversion, in alkali, of $[Fe_4S_3(NO)_7]^-$ into $[Fe_2S_2(NO)_4]^{2-}$,[3] and in fact dilute aqueous alkaline solutions of $[Fe_4S_3(NO)_7]^-$ exhibit[7] ESR spectra characteristic of mononuclear iron-nitrosyl species; similarly oxidative transformation of $[Fe_4S_3(NO)_7]^-$ to $Fe_2I_2(NO)_4$ must involve some form of fragmentation and reformation accompanying the redistribution of the nitrosyl groups.

As part of a broader study[7-12] of nitrosylated iron-sulfur clusters, occasioned partly by their suspected carcinogenicity,[13] we have carried out extended Hückel calculations on several of these systems, in order to shed some light on their transformations, in particular the propensity of the tetranuclear species to undergo significant molecular reorganization as the result of both electron addition and electron removal.

Idealized geometries of C_{3v}, T_d, D_{2h}, and C_{2h} symmetry were employed for $[Fe_4S_3(NO)_7]^-$, $Fe_4S_4(NO)_4$, $[Fe_2S_2(NO)_4]^{2-}$, and the prototype neutral two-iron system $Fe_2(SH)_2(NO)_4$, with dimensions derived from the experimentally determined structures.[1,2,4] I-III are representations of the structures of $[Fe_4S_3$-

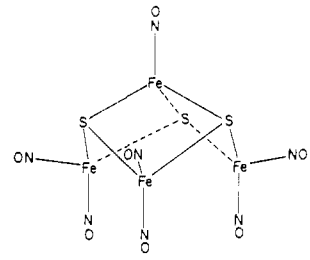

I

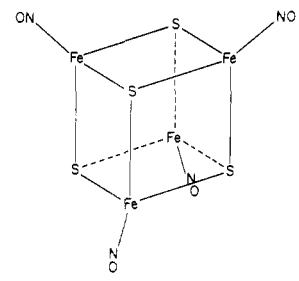

II

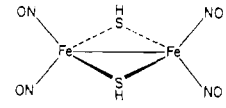

III

(1) Chu, C. T.-W.; Lo, F. Y.-K.; Dahl, L. F. *J. Am. Chem. Soc.* **1982**, *104*, 3409.
(2) Chu, C. T.-W.; Dahl, L. F. *Inorg. Chem.* **1977**, *16*, 3245.
(3) Roussin, F. Z. *Ann. Chim. Phys.* **1858**, *52*, 285.
(4) Thomas, J. T.; Robertson, J. H.; Cox, E. G. *Acta Crystallogr.* **1958**, *11*, 599.
(5) Glidewell, C.; McGinnis, J. *Inorg. Chim. Acta* **1982**, *64*, L171.
(6) Beck, W.; Grenz, R.; Götz, F.; Vilsmaier, E. *Chem. Ber.* **1981**, *114*, 3184.
(7) Butler, A. R.; Glidewell, C.; Hyde, A. R.; Walton, J. C. *Polyhedron*, in press.
(8) Butler, A. R.; Glidewell, C.; Hyde, A. R.; McGinnis, J.; Seymour, J. E. *Polyhedron* **1983**, *2*, 1045.
(9) Butler, A. R.; Glidewell, C.; Hyde, A. R.; McGinnis, J. *Polyhedron* **1983**, *2*, 1399.
(10) Butler, A. R.; Glidewell, C.; Hyde, A. R.; Walton, J. C. *Polyhedron* **1985**, *4*, 303.
(11) Glidewell, C.; Hyde, A. R. *Polyhedron*, in press.
(12) Butler, A. R.; Glidewell, C.; Hyde, A. R.; McGinnis, J. *Inorg. Chem.* **1985**, *24*, 2931.
(13) Wang, G.-H.; Zhang, W.-X.; Chai, W.-G. *Adv. Mass Spectrom.* **1982**, *8B*, 1369.

† Cornell University.
‡ University of St. Andrews.

0020-1669/85/1324-3856$01.50/0